Vibrational Spectroscopy of *N*-Methylacetamide Revisited

W. A. Herrebout, K. Clou, and H. O. Desseyn*

Department of Chemistry, University of Antwerp (RUCA), Groenenborgerlaan 171, B-2020 Antwerpen, Belgium

Received: December 6, 2000

Although a lot of work has been performed on the vibrational analysis of *N*-methylacetamide (NMA), some uncertainties and even contradictions remain, mainly due to the fact that the structure of NMA at room temperature is not stable due to traces of water or due to the fact that the authors only studied the infrared or the Raman spectra. On the basis of the infrared and Raman spectra in the −196 °C to +100 °C temperature range, we have shown that the effects of temperature on the structure and the changes in the strength of the hydrogen bonding within a structure elucidate a lot of the complexity of the solid state vibrational spectra of NMA. Force field calculations on the monomer and multimers ($n = 6$) and solution spectra of NMA and the N-deuterated compound are used to provide a better understanding of the influence of hydrogen bonding on the typical amide fundamentals. Nine typical so-called "amide bands" have been further characterized.

Introduction

The simple peptide *N*-methylacetamide (NMA) has long served as a simple model for understanding the nature of the trans secondary amide function, also called the peptide group.

However, recently developed techniques of UV RR,[1−6] INS,[7−10] gas-phase and force field calculations,[7,11−17] and temperature-dependent spectra[7,8,11,12,14,18−21] illustrated several very unusual features concerning this molecule, especially in the amide A and amide B region (3500−3000 cm^{-1}), the far-infrared region (400−50 cm^{-1}), and the amide I and II region (1700−1500 cm^{-1}) where seven bands have been observed instead of the two known fundamentals.

The conflicting results obtained even in recent studies are very debatable and must be ascribed to an incorrect model and the fact that NMA shows some disorder in the −10 °C to +40 °C temperature region. The spectra of the ordered and disordered crystal cannot be compared, due to the existence of different types of hydrogen bonding. This phenomenon has also been observed in the NMR spectra.[22]

On the basis of the infrared and Raman spectra in the −196 °C to +100 °C temperature range, we will prove in the present paper that the effect of temperature on the vibrational spectra of NMA elucidates a lot of the complexity of these spectra. The main point is that it is very well possible to construct a relatively simple and unambiguous model that is in good agreement with the experiments, instead of the more complicated theories such as proton-transfer, the polaron theory, and Fermi-resonance.

In this article, we also discuss the function of hydrogen bonding in the evolution of the nine typical amide bands, which have been characterized and discussed.

The results obtained in this work go far beyond the initial aim which was to show the effect of variable temperature and pressure on the infrared and Raman spectra of NMA.

Experimental Section

NMA purchased from ACROS ORGANICS was first distilled under vacuum and then dried by freeze-and-thaw under vacuum several times before use.

The infrared spectra were recorded on a Brucker IFS 113v Fourier transform spectrometer, using a liquid nitrogen cooled MCT detector with a resolution of 1 cm^{-1}. For each spectrum, 100 scans were recorded and averaged. The low-temperature measurements were performed with a laboratory designed liquid nitrogen cooled cryostat, consisting of a copper sample holder with a small container that can be filled with liquid nitrogen. This is surrounded by a jacket with KBr windows and placed under vacuum.

From the sample, a pellet in KBr matrix was made under dry nitrogen atmosphere. We recorded far-infrared spectra using a DTGS detector with a resolution of 4 cm^{-1}. For each spectrum, 250 scans were recorded and averaged.

The Fourier transform Raman spectra were recorded on a Brucker IFS 66v interferometer equipped with an FT Raman FRA 106 module. The molecules were excited by the 1064 nm line of a Nd:YAG laser operating at 200 mW. For each spectrum, 1000 scans were recorded and averaged. The low-temperature Raman spectra were recorded on a SPEX 1403−0.85 m double-beam spectrometer. The molecules were excited by a Spectra Physics model 2000 Ar^+ ion laser. A Miller−Harney cell was used to cool the sample. The spectra were recorded with a spectral slit of 4 cm^{-1}. For each spectrum, three scans were recorded and averaged.

The ΔH values were measured on a TA Instruments DSC 2920 equipped with a RCS-cooling system and on a SDT 2960 simultaneous DSC-TGA. The experiments were performed under dry nitrogen atmosphere (50 mL min^{-1}), and the heating rate was 2 °C min^{-1}.

The NMR spectra were recorded on a Varian Unity 400 MHz spectrometer. The chemical shifts are given in ppm. DMSO-d_6 was used as solvent and TMS as internal standard. The concentration was 0.1 M, and data were taken at 30, 60, 90, 120, and 150 °C. The $\Delta\delta/\Delta T$ (ppm/K) was calculated from the shifts.

Computational Details

The density functional theory calculations were performed using GAUSSIAN 98.[23]

10.1021/jp004396c CCC: $20.00
Published on Web 04/26/2001

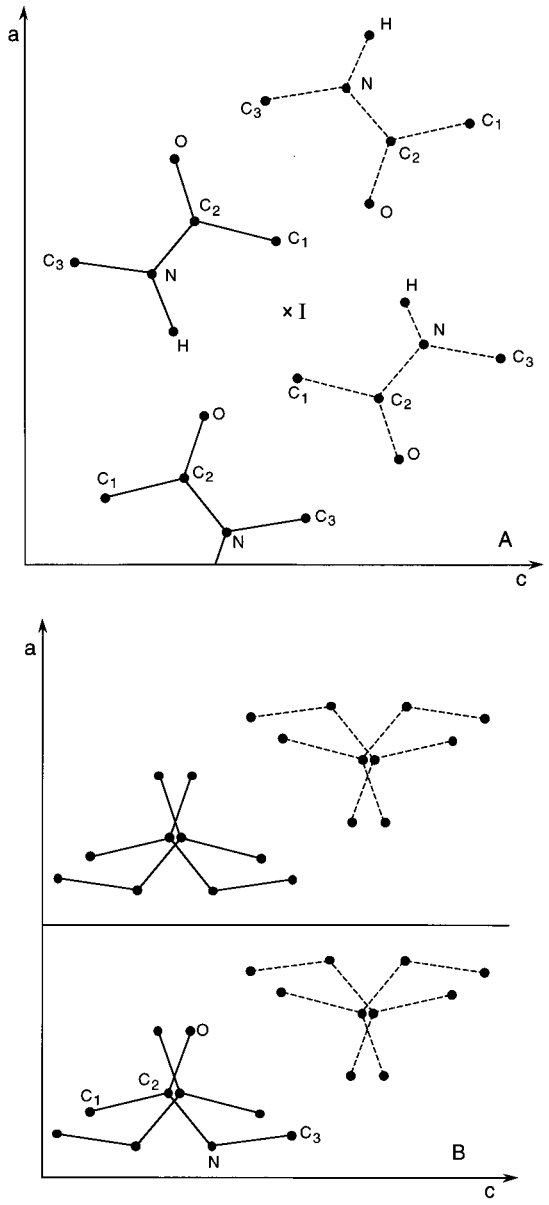

Figure 1. Crystal structure of NMA. (A) Fully ordered form below 10 °C. (B) Partially disordered form above 10 °C, with *a*-axis halved. C_1: $C(CH_3)$, C_2: C(amide), C_3: C(NH). I: Inversion center.

For all calculations, Becke's three-parameter exchange functional[24] was used in combination with the Lee−Yang−Parr correlation functional,[25] while the 6-31G* basis set was used throughout as a compromise between accuracy and applicability to larger systems.

To reduce the errors arising from the numerical integration, the "finegrid" option, corresponding to roughly 7000 grid points per atom, was used for all calculations.

To obtain information about multimers ($n = 2$, 3, 4, 5, and 6), the equilibrium geometry was calculated, without any structural restrictions. Subsequently, for all equilibrium geometries the vibrational frequencies and the intensities were calculated using standard harmonic force fields.

Discussion

1. Geometry of NMA, Phase Transitions. The melting point of NMA is 27 °C, and below 10 °C NMA appears in a fully ordered state and belongs to the orthorhombic space group *Pnmu* (D_{2h}^{16}) with four molecules per unit cell.[26] The planar molecules are parallel to the ac face of the unit cell as given in Figure 1A.

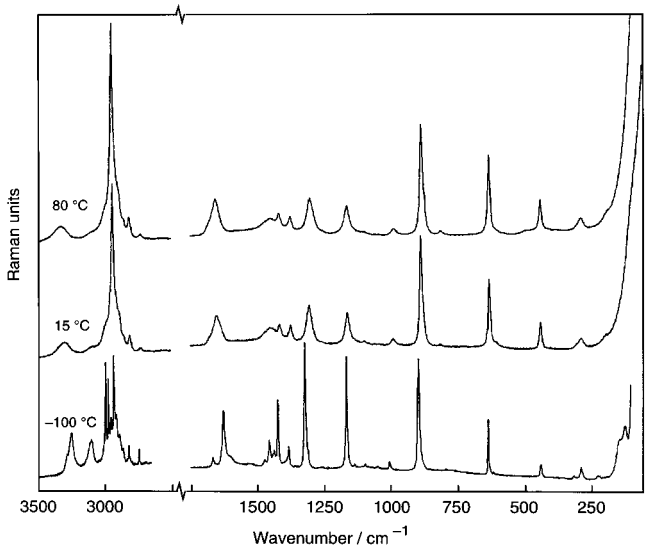

Figure 2. Raman spectra of NMA at 80 °C (A), 15 °C (B), and −120 °C (C).

Between 10 °C and the melting point at 27 °C, hydrogen bonding still exists but the orientation of the NMA molecules is changed drastically.[27] Above the solid transition temperature at about 10 °C, the length of the *a*-axis is halved[26] and each site is occupied at random by a molecule in one of the two orientations as given in Figure 1B. This high-temperature modification is also orthorhombic but contains only two molecules per unit cell.

The Raman spectra at 80 °C, 15 °C, and −100 °C are given in Figure 2. From this figure we can see that the Raman spectrum of the liquid at 80 °C is very comparable with the spectrum obtained at 15 °C and that the small frequency shifts can be explained very well by assuming a stronger intermolecular hydrogen bonding at lower temperatures. The Raman spectrum at −100 °C is very different from the others, mainly due to the crystal effects.

The structure of NMA is unknown at lower temperatures, but we did not observe a phase transition between −10 °C and −80 °C by the DSC measurements. Infrared and Raman spectra taken with an interval of 10 °C between −10 °C and −196 °C have been recorded, and no indication of any transition in this temperature region has been observed. This allows us to conclude that NMA belongs to the same symmetry group in this temperature region.

For better insight into the situation, DSC measurements were performed by heating and cooling the compound between −40 °C and +40 °C.

The DSC curves for heating and cooling are given in Figure 3A,B.

From the heating curve (Figure 3A) at 2 °C/min, we observe a small endothermal process at about 1 °C and several overlapping endothermal processes with a maximum at about 28 °C. The cooling curve (Figure 3B) exhibits a large exothermal peak at about 7 °C and a small exothermal process at −3 °C. For the heating process, we measured 4.7 kJ/mol (±0.5 kJ/mol) for the sum of the phase transition and the melting; for the cooling we measured 5.2 kJ/mol (±0.5 kJ/mol).

The temperature difference (28 °C and 7 °C) is due to the phenomenon of undercooling. The effect of this undercooling is shown in Figure 4, where at a cooling rate of 2 °C/min (given by the full line) we observe an increase of 2.2 °C in 12 s. The heat flow indicated by the dashed line clearly shows this exothermal reaction.

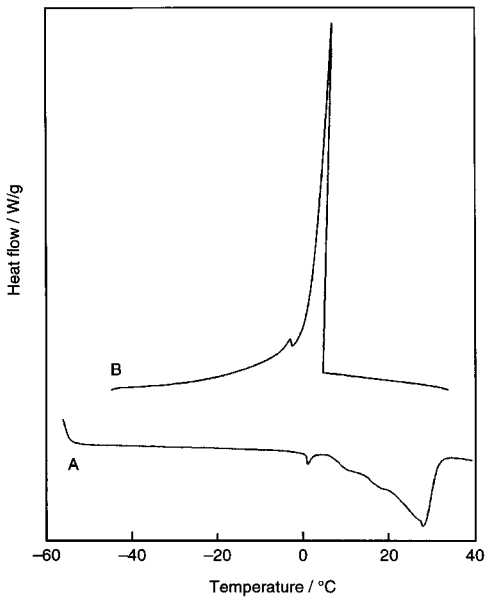

Figure 3. (A) Heating DSC curve for NMA between −40 °C and +40 °C. (B) Cooling DSC curve for NMA between +40 °C and −40 °C.

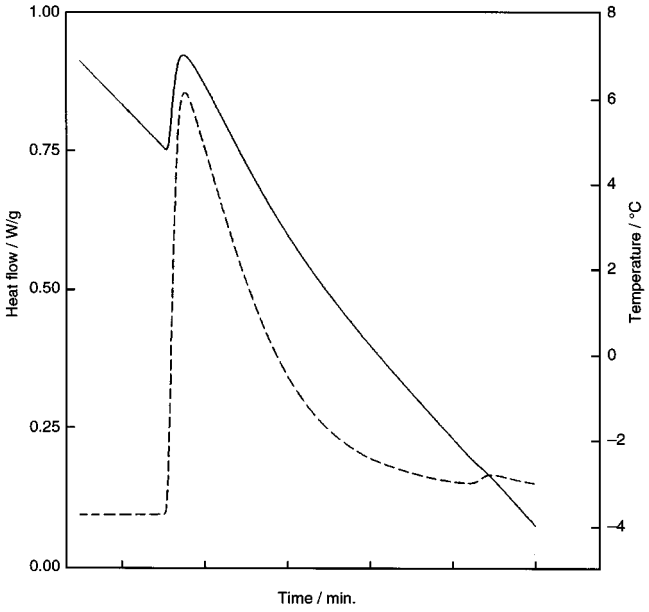

Figure 4. Undercooling in NMA by a cooling of 2 °C/min.

The two small peaks respectively at 1 °C in the heating curve and at −2.85 °C by cooling are probably due to the melting and solidification of traces of water. The DSC curve of the boiling of NMA also exhibits a shoulder at about 113 °C which can be ascribed to traces of water (Figure 5). This uptake of water is practically inevitable as NMA is very hygroscopic, and the water uptake while the DCS cell is being filled is sufficient to observe the traces of water in these DSC curves, although the measurements took place under dry nitrogen atmosphere.

The ΔH_{vap} for NMA has been measured to be 42 kJ/mol (±2). For comparison, we measured the ΔH sublimation of *N*,*N*′-dimethyloxamide, a molecule solely exhibiting two trans secondary amide functions in a normal peptide intermolecular hydrogen bonding with an average N−H···O distance of 2.82 Å[31] (Figure 6). This ΔH_{subl} is measured to be 85 kJ/mol (±2) which is about twice the sum of $\Delta H_{melting} + \Delta H_{vap}$ (4.7 kJ/mol + 42 kJ/mol), indicating a normal intermolecular hydrogen bond strength in both molecules. So the theory of F. Fillaux,[7] considering a proton transfer in a very strong hydrogen bond system, must already be rejected on this basis.

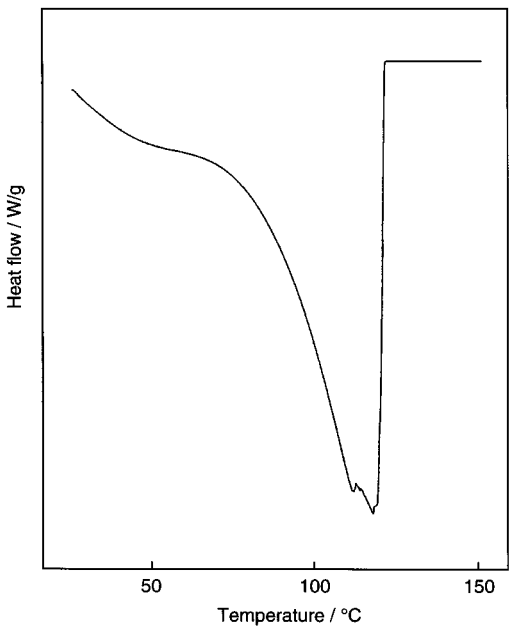

Figure 5. DSC curve for the boiling of NMA.

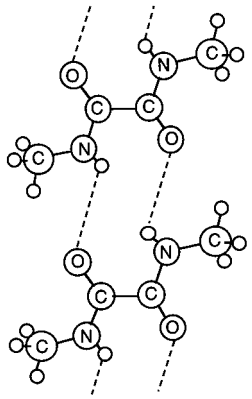

Figure 6. Geometry of *N*,*N*′-dimethyloxamide.

It has to be noted that the energy of the phase transition in NMA is also incorporated in these values.

However, phase transitions in peptide molecules as we observed for *N*,*N*′-diisobutyloxamide at 73 °C and 89 °C, respectively, have an order of magnitude of maximum 1.3 kJ/mol.

Several authors[7,8] already noticed that some amide fundamentals in the spectra at lower temperatures are split into two components. We observed this splitting for practically all in-plane fundamentals of the amide group (see below). This splitting is due to symmetry reasons in the crystal, as by ascent in symmetry from C_s to D_{2h}. We calculated a splitting of each in-plane fundamental (A′) into two different infrared (B_{2u}, B_{3u}) and Raman (A_g, B_{1g}) bands and each fundamental out-of-plane mode (A″) into two Raman bands (B_{2g}, B_{3g}) and one infrared B_{1u} band (A_u mode is not infrared active), according to the following representations:

$$A' \rightarrow A_g + B_{1g} + B_{2u} + B_{3u}$$

$$A'' \rightarrow B_{2g} + B_{3g} + A_u + B_{1u}$$

2. Effect of Hydrogen Bonding on the Amide Fundamentals. The effect of the hydrogen bonding on the amide

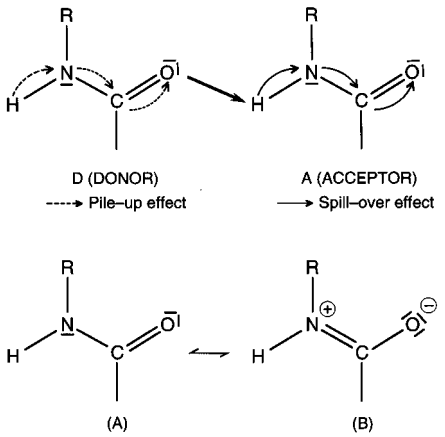

Figure 7. Effect of hydrogen bonding on the amide fundamentals.

fundamentals can be explained by considering this interaction as a donor:acceptor complex according to the theory developed by V. Gutman[32] (Figure 7).

A donor:acceptor interaction results in increasing polarities of the bonds, originating from the donor and acceptor atoms, respectively. The increasing polarity is related to an increase in fractional positive charge at the acceptor atom and an increase in fractional negative charge at the donor atom.

The original loss of negative charge at the donor atom is overcompensated by attracting electronic charge from other parts of the donor molecule to the donor atom. In this way the electron density at the donor atom is increased with appropriate changes of fractional nuclear charges in other areas of the donor molecule. This has been designated as the "pile-up effect" of negative charge at the donor atom.[32b]

The original decrease of fractional positive charge at the acceptor atom is also overcompensated by passing over the negative charges. In this way the fractional negative charges of other nuclei in the acceptor component are increased. This has been designated as the "spill-over effect" of negative charge from the acceptor atoms.[32b]

Both the pile-up and spill-over effects result in the same electron flow and enhance the effect known as the cooperative effect.

The electron flow to more electronegative atoms results in an increased interatomic distance and to a less electronegative atom in a decreased distance.

The change in temperature causes a change in the intermolecular distances[33,34] and consequently a change in the donor−acceptor strength. At lower temperature, we consequently expect a stronger donor−acceptor interaction, resulting in weaker NH and CO bonds and stronger CN bonds.

The hydrogen bonding in secondary amides can also be regarded as a redistribution of electrons in the amide group, due to the lability of the nitrogen lone pair and the high accepting power of the CO group on the other hand, resulting in a greater stabilization of the ionic contribution (B) relative to the normal structure (A) by considering a stronger hydrogen bonding (see also Figure 7). The higher contribution of the ionic form B by stronger hydrogen bonding reduces the CO bond order and increases the CN bond order. The νNH mode is expected to decrease by stronger hydrogen bonding, as the ammonium type of νNH modes (with a partial positive charge on the nitrogen) are always situated at lower frequencies compared with the normal νNH modes.

The electronic distribution in the secondary amide group can be described as resulting from many simultaneous interactions of many factors such as the π-electron delocalization, the inductive effect, the lability of the electron lone pair, changes in hybridization, dipole−dipole interactions, and hydrogen bonding.

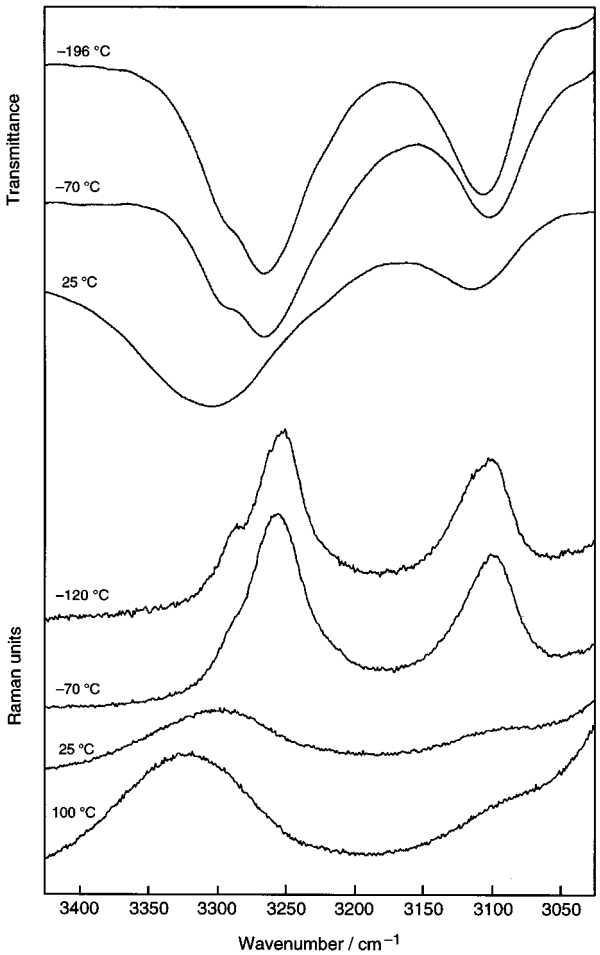

Figure 8. Infrared and Raman spectra of NMA in the 3500−3000 cm^{-1} region at different temperatures.

We observed considerable differences in the amide fundamentals in the gas phase and in the crystal structure at different temperatures. All these frequency shifts on going from the gas phase to the solid, and the shift in the solid at lower temperatures, can be explained very well by considering a stronger hydrogen bonding.

Yet other vibrations such as the CH modes, in which the hydrogen bonding is not participating, remain practically unchanged in frequency. Therefore we believe that, by comparing vibrational solid state spectra at different temperatures, the effect of the change in hydrogen bonding is certainly primordial and explains very well the experimental shifts.

3. Amide A and B Region (3400−3050 cm^{-1}). The Amide A and B region is given in Figure 8 for the infrared and Raman spectra, and Table 1 schedules the frequencies and the proposed assignments in this region. In discussions of secondary amides in this region, it became common to refer to bands at about 3300 cm^{-1} (amide A or νNH modes) and 3100 cm^{-1} (amide B or overtones and combination bands, intensified by Fermi-resonance).

The νNH modes shift to lower frequencies at lower temperatures, as expected for a stronger hydrogen bonding, and clearly show a splitting at lower temperatures as expected in a D_{2h} structure with four molecules per unit cell.

The amide B band shifts to higher frequency at lower temperatures in the Raman spectrum, while this band clearly

TABLE 1: Amide A and Amide B Region (3400−3030 cm^{-1}) (cm^{-1})

T (°C)	+100	+25	−70	−120	−196	Assignment	
Raman	3323 w v br	3300 w br	3287 sh w	3284 sh		νNH (A_g)	Amide A
			3256 m br	3251 m br		νNH (B_{1g})	
	3080 v w	3092 w	3097 m	3099 m		overtones + comb.	
				3108 m		(Amide B)	
Infrared		3304 v br	3287 sh m	3286 sh m	3284 sh m	νNH (B_{2u})	Amide A
			3265 m	3264 m	3263 m	νNH (B_{3u})	
		3114 v br	3101 m	3104 m	3106 m	overtones + comb.	
						(Amide B)	

TABLE 2: *ν*ND Region at −120 °C (cm^{-1})

notation in figure	IR	Raman
band I	2464 w	2467 w
band II	2429 w	2429 w
	2419 w	2418 w
band III	2396 ms	2395 m
band IV	2374 m	2370 ms
band V	2348 mw	2349 mw
band VI	2300 w	2302 w

shifts to lower frequency between the disordered state and the ordered crystal and then shifts, according to the Raman band, to higher frequencies on cooling in the infrared spectra.

The intensity of this band, the asymmetric profile (as can be seen from the Raman spectrum at −120 °C), and the frequency shifts let us conclude that this amide B band must be composed of several overtones and combination bands, enhanced by Fermi resonance. The increased frequencies at lower temperatures indicate that the amide II and III modes, especially (see below), are involved in these overtones and combination bands.

It is well known that the profile of the *ν*NH modes is very complicated[35] and highly temperature sensitive. It is evident that the apparently broad *ν*NH mode is composed of a number of possible sharper bands. This is clearly shown in the *ν*ND region, where the bands appear sharper and where there is no interaction possible with overtones or combination bands of the amide I and II fundamentals. This *ν*ND region (2500−2250 cm^{-1}) is given in Table 2, and Figure 9 gives the infrared and Raman spectra at −120 °C in this 2500−2250 cm^{-1} region.

Instead of the two expected infrared and two Raman modes, six bands are observed, indicated in Figure 9 from I to VI, and band II is split both in infrared and Raman.

The great similarity between the infrared and Raman spectra is very remarkable, and also the regularity in the frequencies can be noticed as the frequency difference between bands II and III, III and IV, and IV and V is about 22 cm^{-1} and the difference between I and II and V and VI is about double (≈45 cm^{-1}).

In fact it may very well be possible that all these bands can be explained as combinations of the genuine *ν*ND modes with a low energy state.[11,36,37]

Recently, H. Ratajczak[38] also studied unusual vibrational properties in hydrogen-bonded systems and concluded that the shape of the *ν*(XH) (or XD) is mainly generated by the mechanical anharmonic coupling between this fundamental and the low frequency (X−H···X) modes of the hydrogen bond system. The author also stated that in the solid state the whole system is further coupled to the bath.

4. Amide I, II, and III Region (1700−1200 cm^{-1}). The 1700−1200 cm^{-1} region of NMA is probably the most discussed and controversial region of any molecule exhibiting a trans secondary amide group.[7,8,11,12,15,16,20,39−53]

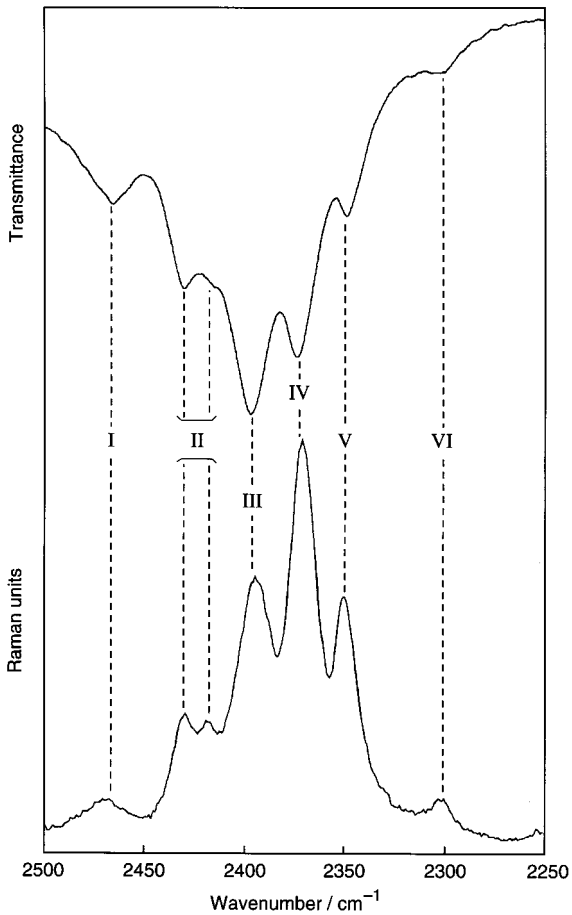

Figure 9. *ν*ND region at −196 °C for the infrared and at −120 °C for the Raman spectrum.

The infrared and Raman bands at low temperature (−196 °C for infrared, −110 °C for Raman) are for the normal and N-deuterated NMA, given in Figures 10 and 11 for this region. In Tables 3 and 4 we scheduled the proposed assignments.

The bands under discussion are indicated from A to J in the tables and the figure for the normal compound, and from A′ to G′ for the deuterated compound.

Band A appears in both Raman and infrared spectra as a weak band at about 1665 cm^{-1}. This band shifts to higher frequency at lower temperature and shifts also to higher frequency on deuteration. This band has certainly no *ν*(C═O) character, as bands with this character are expected to shift to lower frequency at lower temperature and on deuteration. Some authors already

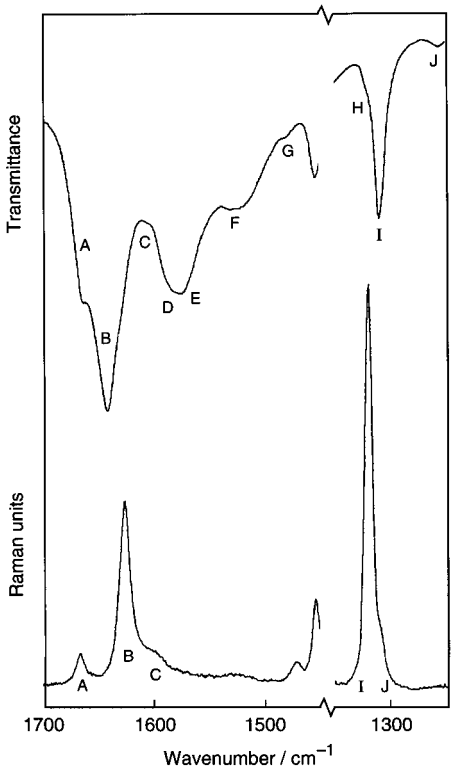

Figure 10. Infrared and Raman spectra at low temperature of NMA in the 1700−1250 cm^{-1} region.

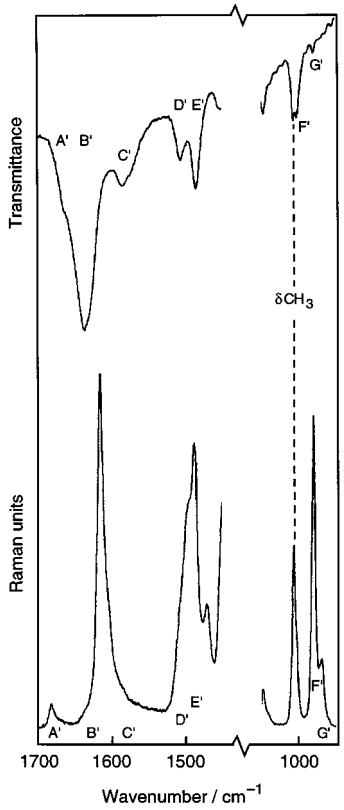

Figure 11. Infrared and Raman spectra at low temperature of NMA-*d* in the 1700−950 cm^{-1} region.

reported on this unconventional supplementary amide band in the Raman spectra at lower temperature,[7,8,12,20] but the corresponding infrared band was not discussed. This band could be due to an interaction between low-frequency modes and other amide fundamentals[11] or, considering the opposite character, to the amide I mode as a result of Fermi-resonance between a combination band and the amide I mode (see below).

TABLE 3: Amide I, Amide II, and Amide III Region (1700−1250 cm^{-1}) for Normal NMA at Lower Temperature (cm^{-1})

notation in Figure 10	IR		Raman		assignment
	−196 °C	−30 °C	−120 °C	−30 °C	
A			1667 (2)	1664 (2)	comb. band
	1663 sh	1659 sh			comb. band
B	1642 vs	1644 vs			am. I (B_{2u})
			1627 (7)	1629 (7)	am. I (A_g)
C	1625 sh				am. I (B_{3u})
			1600 (br 1)		am. I (B_{1g})
D	1586 m		NO		am. II (B_{2u})
E	1576 m	1566 m	NO		am. II (B_{3u})
F	1531 mw	1530 vw	NO		comb. band
G	1484 w		NO		amide cis
H	1325 w		NO		amide cis
I			1320 (10)	1302 (4) br	am. III (A_g)
	1310 s	1301 sbr			am. III (B_{2u})
J			1310 (sh)		am. III (B_{1g})
	1260 w	1256 w			am. III (B_{3u})

TABLE 4: Amide I′, Amide II′, and Amide III′ Bands (1700−950 cm^{-1}) for N-Deuterated NMA (cm^{-1})

notation in Figure 11	IR		Raman		assignment
	−196 °C	−30 °C	−120 °C	−30 °C	
A′			1682 (2)	1679 (2)	comb. band
	1667 sh	1660 sh			comb. band
B′	1638 vs	1639 vs			am. I′ B_{2u}
C′	1633 sh				am. I′ B_{2u}
			1616 (8)	1620 (8)	am. I′ A_g
			1595 sh		am. I′ B_{1g}
D′	1505 m	1497 mw			am. II′ B_{2u}
			1495 sh	1493 sh	am. II′ B_{1g}
			1488 (8)	1486 (8)	am. II′ B_{2g}
E′	1485 ms	1478 mw			am. II′ B_{3u}
	1008 m	1007 m	1008 (3)	1007 (3)	CH def.
F′	1002 ms	997 m			am. III′ B_{2u}
			981 (4)	980 (4)	am. III′ A_{1g}
G′	980 mw	979 mw			am. III′ B_{2u}
			970 (1)	968 sh	am. III′ B_{1g}

The amide I band generally appears in infrared as the most intense amide fundamental and is of medium intensity in Raman. This fundamental has mainly ν(C═O) character and consequently shifts to lower frequency on cooling, due to the stronger intermolecular hydrogen bonding at lower temperature, and also shifts to lower frequency on deuteration, due to the slightly different character of this band in the deuterated compound (see below).

We assigned this amide I fundamental to the intense 1642 cm^{-1} band in infrared, exhibiting a weak shoulder at about 1625 cm^{-1} at lower temperature (bands B and C). The Raman active amide I modes are situated at 1627 cm^{-1}, exhibiting a clear shoulder at about 1600 cm^{-1}.

The splitting of this fundamental, which is expected from symmetry reasons, is better observed for the deuterated compound where we clearly observed two overlapping bands at, respectively, 1638 cm^{-1} and 1633 cm^{-1} in the infrared and at 1616 cm^{-1} and a shoulder at 1595 cm^{-1} in the Raman spectrum (bands B′ and C′). Barthes[8] also observed this weak band at the low-frequency side of the intense amide I and designated this band as band X; other authors[20] suggested that this weak Raman band could be explained in terms of self-trapped states. We, however, think that this weak shoulder in the Raman and the clear splitting of the band in infrared can be ascribed to the predicted splitting in the D_{2h} crystal structure.

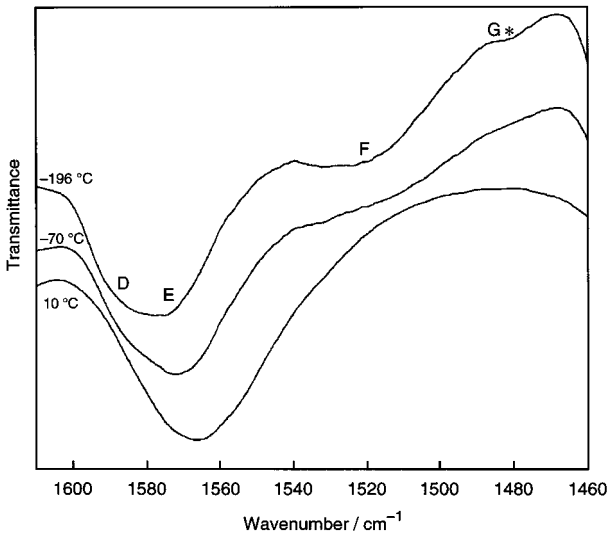

Figure 12. Infrared spectra of NMA at different temperatures in the 1600−1450 cm^{-1} region.

The amide II band is situated in the 1550 cm^{-1} region. In this region we observe a clearly split band (bands D and E in Figure 10) and a weaker and broad band with increasing intensity at lower temperature at about 1530 cm^{-1} (band F in Figure 10). No bands are observed in this region for the Raman spectra.

The bands D and E shift to higher frequencies on cooling and disappear on deuteration as expected for the typical amide II mode. This amide II mode is too weak to be observed in Raman as given earlier by other authors.[7,8,12,20]

The 1531 cm^{-1} band (band F) has been assigned to an overtone of the π(NH) mode (amide V), which increases in intensity on cooling.[11] Figure 12 shows the 1600−1475 cm^{-1} region for the infrared spectrum of the normal product at different temperatures. From this figure, we clearly see the increased frequency of the bands D and E (amide II modes) at lower temperatures, due to the stronger hydrogen bonding; also very obvious is the increased intensity of the band F at 1531 cm^{-1} by lowering the temperature. G. Araki[12] also observed an increased intensity of this 1530 cm^{-1} band by cooling and a decreased intensity of the amide II mode (bands D and E). He stated that there is an isosbestic point between these bands and that the total of integrated intensities of these bands is independent of temperature. This fact strongly suggests that this 1531 cm^{-1} band is related to the amide II fundamental and is interpreted by G. Araki[12] as a coupling between the amide II and lattice phonons. This new quantum state, generated by this coupling, is called a polaron state by analogy with similar electronic excited states.[49] This polaron state is destroyed when many low phonons are excited at higher temperatures, resulting in a lower intensity of this 1530 cm^{-1} band at higher temperatures. It should also be noted that such phenomena are very typical for crystals, such as for NMA, that consist of characteristic one-dimensional chains formed with hydrogen bonds.[12] The first overtone of the amide V (792 cm^{-1} at −196 °C) would be near the amide II. It is very well possible that due to this interaction the amide II band is displaced to higher frequency while the overtone moves down to lower frequency by this Fermi-resonance.[44] So, considering this Fermi-resonance, we would expect a slightly higher amide II frequency compared with other simple secondary amides which do not exhibit this phenomenon.

It is very remarkable that only secondary amides exhibiting the N-CH_3 group show this high amide II mode. F. Fillaux[7] studied the four methyl isotopes of NMA and observed clearly higher amide II frequencies for the N-CH_3 isotopes (1577 cm^{-1} for $CH_3CONHCH_3$, and 1572 cm^{-1} for $CD_3CONHCH_3$) compared with the N-CD_3 isotopes (1562 cm^{-1} for $CH_3CONHCD_3$, and 1558 cm^{-1} for $CD_3CONHCD_3$). Also, for N-CH_3 disubstituted oxamides, a higher amide II mode compared with other alkyl substituents has been observed (Table 5). From this table it is obvious that the mass of the alkyl substituent only plays a minor role in the position of this amide II mode. So, for the bands D, E, and F we can conclude that bands D and E are due to the amide II fundamental and that band F is an overtone of the πNH enhanced in intensity at lower temperature. The high amide II mode observed for amides exhibiting the N-CH_3 group could also be due to an interaction of this amide II with typical frequencies of the N-CH_3 group (hyperconjugation)

TABLE 5: Amide II Infrared Modes for Some Simple Amides (cm^{-1})

compound	amide II (cm^{-1})
$CH_3CONHCH_3$	1577 (ref 7)
$CD_3CONHCH_3$	1572 (ref 7)
$CH_3CONHCD_3$	1562 (ref 7)
$CD_3CONHCD_3$	1558 (ref 7)
RHNCOCONHR	
R = CH_3	1559
R = CD_3	1548
R = C_2H_5	1548
R = C_3H_7	1550
R = cC_3H_5	1542
R = C_4H_9	1557
R = sC_4H_9	1549
R = tC_4H_9	1536

The amide III band is expected as a medium-strong band in infrared and more intense in Raman in the 1250−1300 cm^{-1} region. The infrared and Raman spectra at different temperatures are given in Figure 13 for NMA.

In the infrared spectrum, we observe a broad band at 1301 cm^{-1} at room temperature, a strong band at 1310 cm^{-1} (band I) exhibiting a weak shoulder on the high-frequency side at about 1325 cm^{-1} (band H), and a weak band at 1257 cm^{-1} (band J) at −196 °C. The Raman spectrum exhibits a broad 1302 cm^{-1} band at room temperature and a sharp 1320 cm^{-1} band with a clear shoulder at about 1310 cm^{-1} at lower temperature. These bands shift to higher frequencies on cooling and disappear on deuteration as expected for the amide III modes.

For the deuterated compounds, the coupling between the νCN and δNH is no longer possible, and the amide II′ band, exhibiting more νCN character, is then expected to appear in the 1500 cm^{-1} region, while the δNH mode (amide III′) is situated in the 1000 cm^{-1} region.

Figure 11 shows two infrared bands at 1505 and 1485 cm^{-1} and two Raman bands at, respectively, 1495 cm^{-1} and 1488 cm^{-1}. These bands can undoubtedly be assigned to the four expected amide II′ modes. In Figure 11 we also observe a methyl deformation at 1008 cm^{-1}. In the infrared spectrum, two new bands appear at, respectively, 1002 cm^{-1} and 980 cm^{-1} for the deuterated compound and at 981 cm^{-1} and 970 cm^{-1} in the Raman spectrum. These bands can also easily be assigned to the expected four amide III′ modes (F′ and G′).

It has to be noted, especially for the deuterated compounds, that the splitting of the amide bands is in striking agreement with the structure.

5. Cis−Trans Isomers. *cis*-NMA is estimated to have a higher energy than the trans form by about 10 kJ/mol;[54−56] however, the cis form of some noncyclic proteins has been observed in aqueous solutions by NMR[55,57] and by X-ray crystallography.[58]

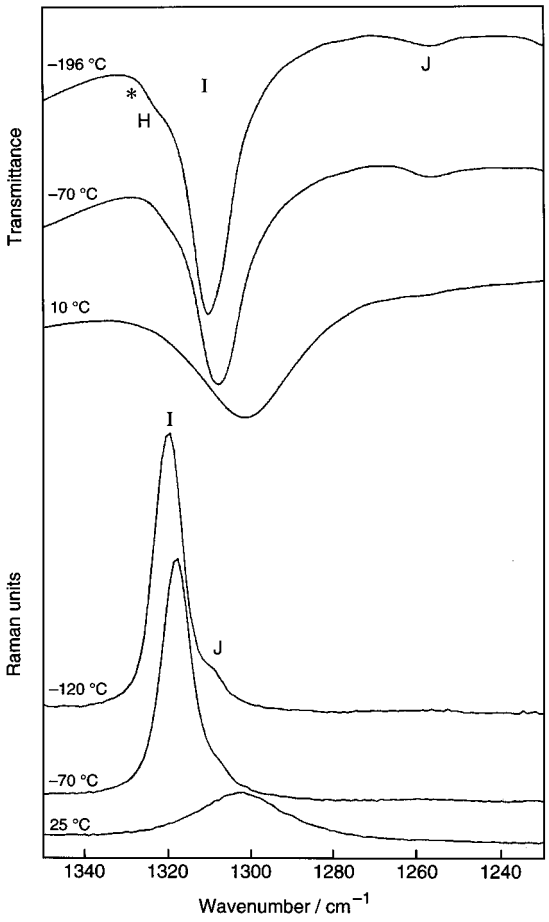

Figure 13. Infrared and Raman spectra of NMA at different temperatures in the 1350−1230 cm^{-1} region.

G. Scherer[59] characterized the cis form by employing NMR techniques in agreement with molecular mechanical calculations and Monte Carlo simulations.[55,56,60] Others[61,62] studied the splitting of the amide I bands as a function of these cis/trans conformations, and 5% *cis*-NMA has been calculated in diluted CCl_4 from splitting of the νNH modes[63] or the νCO overtones.[64]

It is very well known[61,65,66] that the abundance of cis and trans isomers of the noncyclic amide groups depends mainly on the size and sterical influence of the neighboring alkyl substituents. The steric interaction between the *N*-alkyl substituent and the carbonyl oxygen atom appears to be the main reason that some of the molecules exhibit cis character. However, when the *N*-alkyl substituent becomes sufficiently large (*tert*-butyl), an additional steric interaction occurs with the *N*-alkyl group on the α-position of the secondary amide, and the molecule then reverts to the trans position.

S. Ataka[54] studied the cis/trans equilibrium of NMA by matrix isolation and identified two bands of comparable intensity in the cis form, completely different from the position of the typical trans bands at, respectively, 1485 cm^{-1} (νCN) and 1325 cm^{-1} (δNH). In the cis form, the coupling between νCN and δNH is much less than for the trans conformation, resulting in these two new bands.

In Figures 12 and 13 we marked two weak bands with an asterisk (see also band G and H in Figure 10), these bands appear as weak infrared bands at 1484 cm^{-1} (Figure 12) and as a shoulder of the more intense amide III band at about 1325 cm^{-1} (Figure 13) at lower temperature. We strongly believe that these weak bands could be due to two fundamentals of the cis form in the solid state. However, no other bands could be assigned for this cis form as all other fundamentals practically coincide with the fundamentals of the trans form. For the N-deuterated NMA, all cis and trans fundamentals practically coincide, so no vibrational evidence for the presence of the cis form in the deuterated compound could be given.

6. Amide S Band. UV RR[54] of secondary amides exhibit an extra band at ca. 1390 cm^{-1}, this additional band, intensified by UV RR, could not be assigned to a previously known amide vibration and is called the amide S band.

This amide S band only occurs for amides exhibiting H atoms attached to the (C)Cα atom. This 1390 cm^{-1} band is not present in the CD derivatives, where an upward shift and intensification of the amide III band is observed compared to the CH compound.[7,54,1]

The origin of this band is very contentious and could be due to an overtone of the amide V, which gains intensity via the amide III mode,[54] or by torsional displacement in the excited state.[6]

Fillaux[7] studied the methyl isotopes of NMA and observed this amide S band at 1384 cm^{-1} for CH_3-$CONHCH_3$ and at 1396 cm^{-1} for CH_3-$CONHCD_3$; for these isotopes the amide III band is observed at 1320 cm^{-1}. The amide S band has not been observed for $CD_3CONHCH_3$ and $CD_3CONHCD_3$, and for both isomers the amide III band is situated at 1348 cm^{-1} (i.e., 28 cm^{-1} higher than for the $C(CH_3)$ isomers).

The fact that this amide S is not observed for the N-deuterated compounds lets us conclude that this amide S band also could originate from an interaction of the amide III with the δ_sC-(CH_3) mode (calculated at 1354 cm^{-1}, see below). Torii[72] assigned the amide S band to the 1377 cm^{-1} in NMA and to the 1371 cm^{-1} band for NMA·$3H_2O$.

We observed no evidence in the infrared and in the Raman spectra of this amide S band, which can be intensified by UV RR.[54]

7. Amide IV to VII Bands for NMA. The bands observed at different temperatures in infrared and Raman are for the 900−400 cm^{-1} region given in Table 6.

In this region we observe the secondary amide fundamentals designated as the amide IV to VII bands. All these fundamentals can be described as "localized frequencies" and appear in a broad region with rather variable intensity, generally due to coupling with other deformations of functional groups on the Cα atom. These bands are, considering the region and the variable profile, not useful for diagnostic purposes.[55,65] In this region we should observe the four amide fundamental deformations and the νCC mode.

All secondary amides, except the formamides, exhibit a band in the 850 cm^{-1} region and a second band in the 600 cm^{-1} region. Both bands appear as polarized bands in the solution spectra and must consequently be due to in-plane modes. These bands are in the literature generally designated as a νCC, for the band in the 850 cm^{-1} region, and as the amide IV with mainly δNCO character in the 600 cm^{-1} region. The PED values in most force field calculations clearly show a strong coupling between the νCC and the δNCO modes. The PED distribution depends on the nature of the substituent on the α-C atom and the method of calculation. So both bands are typical for the secondary amide function and can consequently be designated as typical amide bands. So we propose to call these bands the amide IVa and amide IVb bands, as only one amide deformation is considered in these two fundamentals.

The amide VI bands with mainly out-of-plane deformation NCO character are also generally observed in the 600 cm^{-1}

TABLE 6: Amide IV to VII Band Assignments for NMA (cm^{-1})

normal				deuterated				
IR		Raman		IR		Raman		
25 °C	−196 °C	25 °C	−120 °C	25 °C	−196 °C	25 °C	−120 °C	assignments
892	894	883	894	880	882	879	883	amide IVa
725	792	−	790	520	557	−	560	amide V
629	636	628	635	627	636	627	633	amide VI
	629				629			
602	614	609	616	599	614	−	−	amide IVb
439	440	437	439	440	441	436	436	amide VII

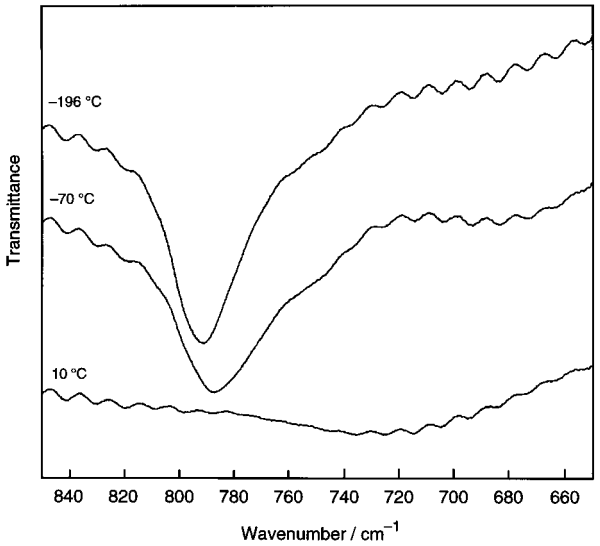

Figure 14. Infrared spectra of NMA at different temperatures in the 850−650 cm^{-1} region.

region, and force field calculations sometimes indicate this amide VI band at slightly higher frequency than the amide IVb band.

The only way to differentiate between these fundamentals is the difference of polarization of the two bands: one fundamental (amide IVb) is a deformation in the plane of the amide group, and consequently totally symmetric to this plane, while the other fundamental is not symmetric and appears less polarized.

The amide V band generally appears as a broad band at room temperature in the 700−750 cm^{-1} region and shifts to the 500−550 cm^{-1} region on deuteration. This band entails a high πNH character and becomes smaller and shifts to higher frequencies on cooling, as can be observed in Figure 14. This amide V band has, for NMA, been observed by H. K. Kessler[21] who already commented on its breadth.

The unusual large breadth of this band at room temperature, compared with other simple secondary amides, is certainly due to the disorder in the structure at room temperature, resulting in a heterogeneity of hydrogen bond interaction. The strong shift to higher frequencies on cooling depends mainly on the hydrogen bond strength, which is very well comparable with other secondary amides, and to the lattice contraction with temperature,[67−69] which must be significant considering the great frequency shift.

Other authors[8] also observed a splitting of the bands in the 600 cm^{-1} region, which is less pronounced for the lowest band. This splitting is, as mentioned earlier, due to the crystal structure.

The amide VII band, which generally entails a high in-plane NCO character, is generally observed in the 450 cm^{-1} region and can, for NMA, undoubtedly be assigned to the 439 cm^{-1} band.

It must also be noted that all these modes shift to higher frequencies by cooling, as is expected for a stronger hydrogen bonding at lower temperature due to the lattice contraction.

8. Far-Infrared Region. The far-infrared region has extensively been studied by INS, vibrational spectroscopy, and force field calculations.[7,18,19,27,39,70,71]

In this region, we expect possible other amide fundamentals, the intermolecular modes, and the external modes. The proposed assignments are given in Table 7 for the normal and deuterated compound at different temperatures.

T. Miyazawa[17] assigned, in an earlier work, the amide I to VII modes as a fingerprint for the secondary amide, assuming that there were no internal fundamentals below 300 cm^{-1}, except the methyl torsion modes.

However, recent results by other authors, as well as our calculations (see below) and the experiments, locate a typical amide band with high δNH, δNCO, and ρNCO character in the 300 cm^{-1} region. This fundamental amide VIII band shifts as expected to higher frequency on cooling and is practically not influenced by deuteration. The splitting of this fundamental due to the crystal effect is obvious at lower temperatures, as can be observed from Figure 15 exhibiting the infrared and Raman spectra at different temperatures in the 350−175 cm^{-1} region.

In the solid state spectra we also have to consider the intermolecular modes which describe the different intermolecular vibrations involving the hydrogen bonding.[72] The highest of these frequencies is the ν_σ or the intermolecular stretching mode ν_σ(N−H···O) which appears as a broad band situated in the 160−200 cm^{-1} region.[73] The other modes described as the intermolecular deformations must be situated at lower frequencies. The position of this ν_σ mode is mainly determined by the mass of the donor and the acceptor (the nitrogen and the oxygen atoms) and the strength of the intermolecular hydrogen bonding. The effect on deuteration is rather small compared with the normal NH/ND ratio.

F. Fillaux[19] calculated an internal torsion mode around an axis close to the CN bond of the amide in the 200 cm^{-1} region; also, our calculations (see below) predict a fundamental exhibiting τCN character in the 200 cm^{-1} region. This typical amide fundamental can be regarded as the amide IX band.

The broad bands arising at 198 cm^{-1} in the infrared and at 188 cm^{-1} in the Raman spectrum shift considerably to higher fequency on cooling and exhibit at least two bands at lower temperature as can be observed in the low-temperature infrared spectrum. So in this 200 cm^{-1} region we can expect two bands, assigned, respectively, to the amide IX and the ν_σ(N−H···O).

All secondary amides exhibit a band in the 100−120 cm^{-1} region due to a vibration involving the atoms within the hydrogen bond.[2] K. Itoh[27] performed a normal mode calculation in terms of linear structures, neglecting interactions between chains. The normal mode calculated at 124 cm^{-1} shows the amplitudes of the atoms involved in the hydrogen bonding to

TABLE 7: Far-Infrared Region for NMA (cm^{-1})

Normal						Deuterated						Assignments
I.R.			Raman			I.R.			Raman			
25°C	−70°C	−196°C	25°C	−50°C	−100°C	25°C	−70°C	−196°C	25°C	−50°C	−100°C	
290	305	318	286	316	316	288	303	394	284	313	313	Amide VIII
	287	288		289	289		284	285		286	286	
198	203	221	188 br	221	224	196	215	215	186 br	218	222	ν_σ(N–H·····O)
	203	216					209	209				Amide IX
108	119	123	121	124	140	108	114	119	120 sh		130 sh	ν_γ(N–H·····O)
					121					122	121	skel. mode
			95	98	99				97	97	99	skel. mode
81	84	88	77	76	86	81	82	84	76	76	88	ν_β or ν_α(N–H·····O)
					74						77	skel. mode

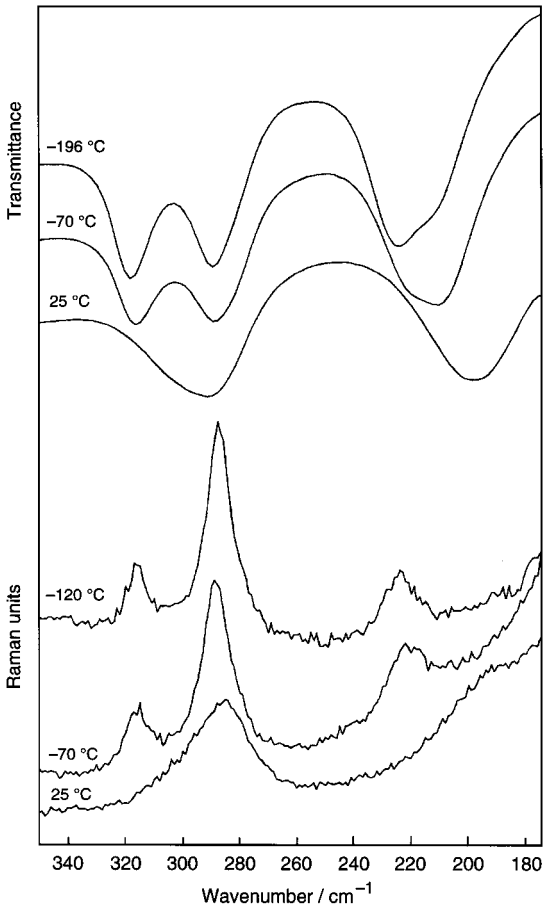

Figure 15. Infrared and Raman spectra of NMA at different temperatures in the 350−175 cm^{-1} region.

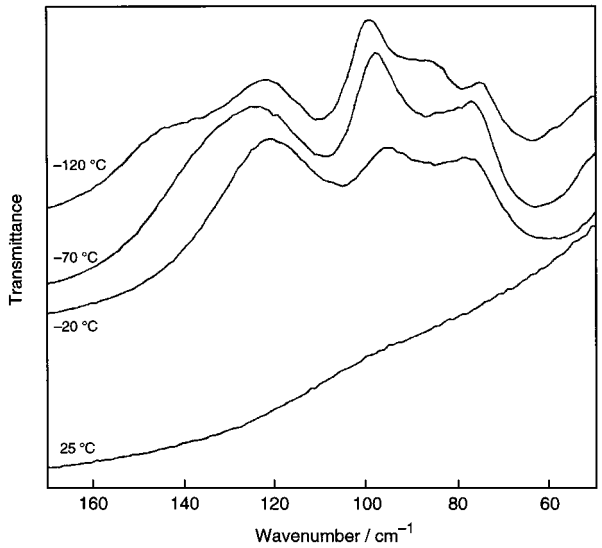

Figure 16. Raman spectra of NMA at different temperatures in the 170−50 cm^{-1} region.

be perpendicular to the molar planes and in opposite phases in different molecules. This mode can consequently be described as the out-of-plane intermolecular deformation mode (ν_γ).

Figure 16 shows the Raman spectrum in the 175−50 cm^{-1} region at different temperatures. From this figure we can see that the low-frequency modes are not observed at 25 °C, but at −20 °C we can distinguish three rather broad bands at, respectively, 121, 95, and 77 cm^{-1}. The 121 cm^{-1} band clearly splits in two bands observed at 140 cm^{-1} and 122 cm^{-1} at −120 °C, the 95 cm^{-1} shifts to 99 cm^{-1} on further cooling, and the 77 cm^{-1} band also shows a splitting in a 75 cm^{-1} band and a 86 cm^{-1} band. Two bands, one shifting from 121 cm^{-1} to 140 cm^{-1} and the other shifting from 77 cm^{-1} to 86 cm^{-1}, appear very sensitive to lattice contractions and can be assigned to deformation modes involving the (N−H···O) system. The highest band can be assigned to the predicted out-of-plane intermolecular mode,[27,33,34] while the 77 cm^{-1} band shifting to 86 cm^{-1} on cooling could be ascribed to the ν_β or ν_α mode of the intermolecular deformations.

The other modes (122, 99, and 75 cm^{-1} at −120 °C) are practically not influenced by the temperature and can be described as skeletal modes.

9. Solution Spectra. The solution spectra of secondary amides have been discussed by several authors.[71,76] In very diluted solvents, where no solute:solvent hydrogen bonding occurs, NMA molecules do not form hydrogen bonds and the spectrum of the monomer can then be observed. However, in more concentrated solutions, aggregates and associates of molecules are formed, first by dimers and then trimers. An increase in concentration shifts the equilibrium to the formation of higher multimers. Bands such as the CH_3 modes are hardly influenced; this suggests that when hydrogen bonding is changed, a redistribution of the electron density takes place practically strictly within the (HNCO) group.

Figure 17 shows the 3500−3200 cm^{-1} region in the infrared at different concentrations of NMA in CH_2Cl_2. For the saturated

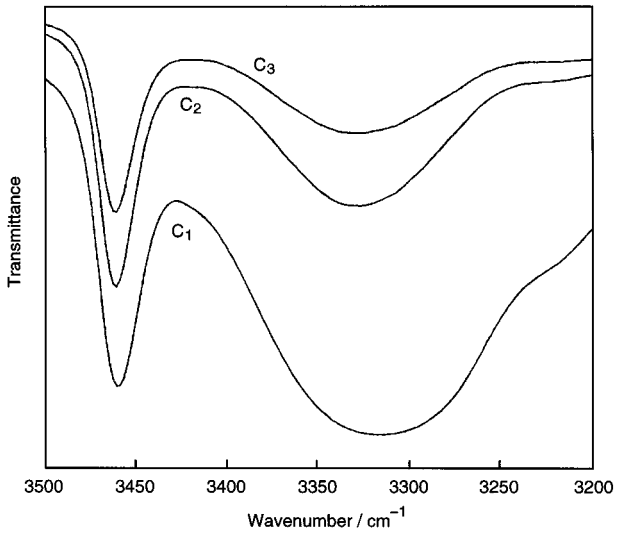

Figure 17. CH_2Cl_2 infrared solution spectra of NMA at different concentrations ($C_1 > C_2 > C_3$).

TABLE 8: Solution Spectra of NMA (cm^{-1})

CCl_4				
IR dil.[70]	Ram. conc.	H_2O conc. → dil.	D_2O conc. → dil.	assignments
3476	3299	3302−3308−3314		νNH
			2408 → 2414	νND
1700	1652	1651−1658−1626	1650−1652−1626	amide I, amide I′
1500	−			amide II
1260	1303	1301−1305−1315		amide III
			969 → 966	amide III′
	883	881−882−884	871	amide IVa

solution we observe a sharp separated band at 3460 cm^{-1}, due to the monomer,[71] and a more intense and very broad band with a maximum at about 3310 cm^{-1} arising from a superposition of different multimers.[71]

By dilution we observe consequently more free molecules as the relative intensity of the 3460 cm^{-1} band becomes more intense compared to the broad 3310 cm^{-1} band. We also observe a shift to higher frequency of this broad band (from 3310 to 3329 cm^{-1}) due to the increasing number of shorter associates by dilution.[83]

From Table 8, we can see that the data observed in diluted CCl_4 solutions are very close to the calculated values of the monomers. In the concentrated CCl_4 solutions in the Raman spectra, we observe data closer to the multimers as expected, as the hydrogen bonding shifts the νNH and amide I bands to lower frequencies and amide II and III bands to higher frequencies.

Table 8 also gives the Raman data of dilution in H_2O. H. Torii[75] studied the effect of hydration on NMA and showed that the frequencies are strongly affected by both the dielectric effect and the formation of different hydrogen bonds from pure amide:amide to amide:$3H_2O$ clusters on dilution.

The effect of NMA−water hydrogen bonds on the vibrational spectra were examined by explicity including water molecules in the MO calculations, i.e., two water molecules to the lone electron pairs of the CO groups and one water molecule to the NH group,[77,78] as given in Figure 18. The dominance of the species with three hydrogen-bonded water molecules has also been shown in a Monte Carlo simulation.[79]

J. B. O. Mitchell[80] performed Hayes−Stone intermolecular perturbation theory[81] calculations on amide:water complexes. The different interactions and the calculated energies are

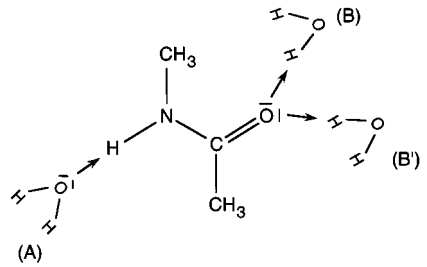

Figure 18. NMA·$3H_2O$ system.

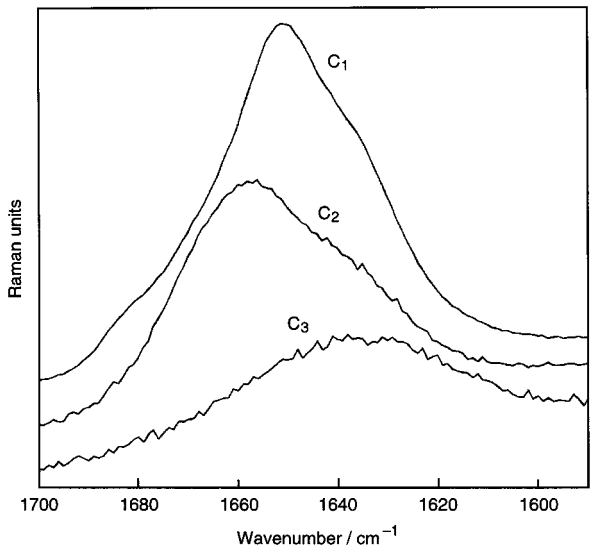

Figure 19. Water Raman solution spectra of NMA at different concentrations ($C_1 > C_2 > C_3$).

schematically given in Table 9. From these data they concluded that the change in the intermolecular interaction energy associated with the hydrogen bond exchange process is small (less than 5 kJ/mol). They also concluded that the amide:amide hydrogen bonds and the interaction with water should be approximately isoenergetic.

The factors determining the H-bond energy of NMA in H_2O are far more complex than those governing this model, as it is well known that the intrinsic stability of the interpeptide bond in water is very small and that these interamide hydrogen bonds do not form until the solute concentration is very high.[81,82]

So, the first change in the hydrogen bonding of NMA on dilution in water is the breaking of the amide:amide system which on the NH side is replaced by the amide:water interaction (water molecule A in Figure 18). This slightly weaker hydrogen bonding (see Table 9) results in a decreased νNH frequency on dilution.

The Raman spectrum of the amide I region on dilution is given in Figure 19. From this figure we clearly see that at the first dilution we observe an increase of this band, resulting in a broad band with a clear shoulder on the low-frequency side. The high-frequency band disappears on further dilution, and the shoulder at the low-frequency side becomes more intense. This is unexpected considering the νNH shift on dilution but can very well be explained by considering a stronger water:amide interaction by dilution (see Table 9).

The slight upward shift at the beginning can be explained by assuming a water:amide interaction with one molecule of water per amide unit. The decrease in frequency is then the formation of the second water:amide hydrogen bonding on further dilution.

The amide III band exhibits great νCN character. The electronic distribution on dilution mainly occurs in the NCO

TABLE 9: Hydrogen-Bonding Energies in the NMA:Water System (kJ/mol)

Amide : Amide	N—H	⇐	O=C	−21.97
Amide : water	N—H	⇐	O(H)H	−18.82
water : Amide	H(O—H)	⇐	O=C	−25.98
water : water	H(O—H)	⇐	O(H)H	−20.35

amide group, so a lowering of the amide I band, with mainly νCO character, suggests an increase in the electron density of the CN of the amide group, resulting in a higher νCN mode.

The decrease of the band with high νCO character and the increase of the band with mainly νCN character on dilution are also reflected in the interatomic distances of NMA and the NMA·3H_2O cluster (for NMA: CO 1.2043 Å, CN 1.3495 Å and for NMA·3H_2O: CO 1.2214 Å and CN 1.3316 Å).[75]

In D_2O we observe an increase of the νND, a decrease of the amide I′, and an increase of the amide II′, with high νCN character. The δND (amide III′) hardly shifts on dilution to lower frequency, as can be expected for a weakening of the ND hydrogen bonding.

In the present and previous studies of water, NMA systems show that the hydrogen bonding is very complex and may not easily be reduced to a simple model. G. Chen[84] also calculated that NMA and its hydrogen-bonded water molecules are vibrationally coupled.

10. Force Field Calculations. Since the first study of Miyazawa,[17] different force fields have been proposed,[7,13−16,54] and practically all force fields are very comparable in the high-frequency region, except the assignment scheme as proposed by F. Fillaux.[7] These authors made the assignment in terms of a dynamical proton exchange between the amidic (OCNH) and imidolic (HONC) forms in infinite chains of hydrogen-bonded molecules. This proton transfer is described by a symmetric double-minimum potential function. In this study the νNH has been assigned to the 1575 cm^{-1} band, and the 3250 cm^{-1} band has been assigned to the first overtone of the amide I fundamental. This unreasonable low-frequency for the νNH mode was interpreted as a strong NH bond weakening by proton transfer to the neighboring oxygen. This interpretation is wrong as can be shown by structural, thermodynamical, and spectroscopic arguments. A. Lautié[31] studied the relationship between the νNH modes and the N···O distances in crystals exhibiting N−H···O hydrogen bonds and concluded an "average" hydrogen bonding for NMA considering the N−H···O distance of 2.825 Å.[26] Our measurements on the ΔH_{vap} of NMA (42 kJ/mol) clearly show that we must consider a normal peptide bond for NMA, and spectroscopic arguments also make the assignments by Fillaux[7] and Kearly[85] very questionable.

The infrared and Raman spectra of NMA discussed in this article are typical for a normal secondary amide and exhibit the expected characteristic amide bands. Furthermore, as we already clearly indicated, we definitely observed the νND mode in the 2450 cm^{-1} region, which cannot exist if there were no νNH bonds in the normal compound in the expected 3300 cm^{-1} region.

C. L. Perrin[86] also stated that the position of the hydrogen being equally likely on the nitrogen and the oxygen is practically impossible due to the great difference in energies (4 kJ/mol) of the two resonance forms. Other arguments, especially on the

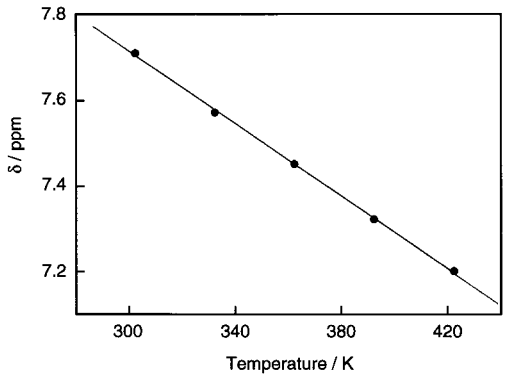

Figure 20. NH−NMR signal as a function of temperature.

overtones and the intensities of these bands,[87] confirm the improbability of these alternative assignments. H. Kessler[88] concluded from an NMR temperature gradient study that the chemical shift of the NH signal in peptides is in excess of 4×10^{-3} ppm/K for normal peptide intermolecular hydrogen bonds; we obtained a value of 4.23×10^{-3} ppm/K for NMA (see Figure 20), confirming the normal peptide bond in NMA.

We mostly agree with the characterizations of the amide fundamentals in the high-frequency region as calculated by other authors, and the CH_3 assignments are in good agreement with the data given by E. M. Bradbury.[11] The differences in the low-frequency region will be discussed later in the article.

Since ab initio calculations refer to an isolated molecule it would be appropriate to compare the calculated frequencies with the gas-phase frequencies, but these data are not of high enough quality at the present time. However, the N_2 and Ar matrix spectra do contain this level of detail, although these frequencies are shifted slightly compared to the gas phase,[89] indicating some interaction between NMA and the matrix. Therefore, the calculated frequencies and their PED values are compared with the data of the matrix spectra[54] and are given in Table 10 for the normal compound. Table 11 exhibits the data for the deuterated NMA compared with the normal compound.

Because well-known[90] frequencies calculated with ab initio force constants are 10−20% higher than the experimental frequencies, primarily due to limitations in the basis set and the neglect of electron correlation, we scaled the force constants to reproduce the observed frequencies of the CH_3 modes, as these modes are less sensitive to aggregations and hydrogen bonding.

As the presented force field can be regarded to be very reliable, it can be used to characterize the amide fundamentals and to discuss the influence of the hydrogen bonding on the fundamentals.

In their first analysis of the infrared spectra of NMA, T. Miyazawa[17] identified seven bands between 2000 and 170 cm^{-1} as vibrations within the trans secondary amide entity. These bands are traditionally referred to as amides I to VII for the normal and I′ to VII′ for the N-deuterated compounds.[65]

The amides I, II, and III bands are well assigned and characterized, and our calculations are in good agreement with the literature. The amide fundamentals in the lower frequency region are less identifiable and need more reconsideration.

Table 12 schedules the characteristic amide bands, the gas-phase frequencies for the monomer and multimers, and the frequencies of the solid state at room temperature and at −196 °C. Regarding the sequence, gas-phase monomer → gas-phase hexamer → solid state at 25 °C → solid state at −196 °C, we expect stronger intermolecular hydrogen bonding. These fre-

TABLE 10: NMA Fundamentals (Gas Phase) (cm^{-1}): Calculated Frequencies and PED Values

obsd[54]	calcd[a]	PED (%)	assignments
3498	3456	100 νNH	νNH
3008	3016	68 $\nu_{as}CH_3(N)$ + 22 $\nu_{as}CH_3$	
3008	2985	76 $\nu_{as}CH_3(C)$+ 24 $\nu_{as}CH_3(C)$	
2973	2981	74 $\nu_{as}CH_3(C)$+ 23 $\nu_{as}CH_3(C)$	
2915	2939	74 $\nu_{as}CH_3(N)$ + 25 $\nu_{as}CH_3(N)$	
2915	2910	98 $\nu_{s}CH_3(C)$	
	2892	90 $\nu_{s}CH_3(N)$	
1707	1702	77 νCO + 7 νCN + 4 ρNCO	amide I
1511	1502	42 δNH + 16 νCN + 14 δNR	amide II
1472	1454	70 $\delta_{as}CH_3(N)$ + 23 $\delta_{as}CH_3(N)$	
1446	1446	34 $\delta_{as}CH_3(N)$ + 20 $\delta_{as}CH_3(C)$ + 11 $\delta_{as}CH_3(N)$ + 9 δNH	
1432	1439	35 $\delta_{as}CH_3(C)$ + 16 δNH + 14 $\delta_{as}CH_3(N)$ + 12 $\delta_{as}CH_3(C)$	
1419	1426	68 $\delta_{as}CH_3(C)$ + 23 $\delta_{as}CH_3(C)$	
1370	1384	85 $\delta_{s}CH_3(N)$	
1370	1354	86 $\delta_{s}CH_3(C)$	
1266	1219	27 δNH + 21 νCN + 15 δNR + 9 δNCO + 8 νCC	amide III
1168	1120	45 $\rho_{as}CH_3(N)$ + 15 $\rho_{as}CH_3(N)$ + 13 δNH + 8 νNR	
1089	1106	69 $\rho_{as}CH_3(N)$ + 23 $\rho_{as}CH_3(N)$	
1089	1069	60 νNR + 10 $\rho_{as}CH_3(C)$ + 8 νCC	
1037	1013	54 $\rho_{as}CH_3(C)$ + 18 $\rho_{as}CH_3(C)$ + 16 πCO	
980	954	38 $\rho_{as}CH_3(C)$ + 22 νCC + 12 $\rho_{as}CH_3(C)$+ 8 νNR	
857	831	26 νCN + 16 δNR + 14 νCC + 12 δNCO	amide IVa
658	601	64 πCO + 15 τCN + 14 $\rho_{as}CH_3(C)$	amide VI
619	593	40 δNCO + 30 νCC + 16 δNR	amide IVb
439	414	45 τCN + 27 πNH + 20 πCO	amide V
	412	68 ρNCO + 10 δNR + 9 $\rho_{as}CH_3(C)$	amide VII
	276	57 δNR + 21 δNCO + 18 ρNCO	amide VIII
	154	67 πNH + 23 τCN	amide IX
	71	51 τNR + 13 πNH + 9 τCN	
	45	62 τCC + 12 πCO + 7 τNR	

[a] Correction factor = 0.95.

quency shifts can all be very well explained solely by assuming a change in the hydrogen-bonding strength.

The fact that all fundamentals obey this sequence allowed us to conclude that the PED values for the monomer, the multimers, and the solid state must be very well comparable except for the amide V and amide VI bands where a visualization of the modes in the hexamer clearly shows more πCO character for the amide V and πNH character for the amide VI mode.

This is not unusual, as we observed opposite shifts for the $\rho_{as}NH_2$ and $\omega_{as}NH_2$ mode for urea, and the PED data in the gas phase and in the solid state were indeed calculated to be very different.[91]

11. Amide I to IX Bands. The band arising in the 3400 cm^{-1} region shifting to lower frequency by stronger hydrogen bonding and appearing in the 2500 cm^{-1} for the N-deuterated compound has pure νNH/ND character. The ratio νNH/νND = 1.364 confirms this pure character.

The amide I band shifts to lower frequency on cooling and is practically not influenced by deuteration. The PED values for the normal and deuterated compounds are practically identical, and the contributions in the PED data are all due to vibrations within the amide group.

The amide II and amide III modes both have high νCN and δNH character. For bands with high νCN character and also with δNH character we expect an increased frequency by stronger hydrogen bonding. The amide II band is situated in the 1550 cm^{-1} region and the amide III in the 1220 cm^{-1} region;

TABLE 11: NMA(D) Calculated Fundamentals and PED Values

NMA (H) calc. (0.95)	NMA (D) calc. (0.95)	PED (%)	assignments
3456			νNH
3016	3016	68 $\nu_{as}CH_3(N)$ + 22 $\nu_{as}CH_3(N)$	
2985	2985	76 $\nu_{as}CH_3(C)$ + 24 $\nu_{as}CH_3(C)$	
2981	2980	74 $\nu_{as}CH_3(C)$ + 23 $\nu_{as}CH_3(C)$	
2939	2939	74 $\nu_{as}CH_3(N)$ + 25 $\nu_{as}CH_3(N)$	
2910	2910	98 $\nu_{s}CH_3(C)$	
2892	2892	90 $\nu_{s}CH_3(N)$	
	2533	98 νND	νND
1702			amide I
	1698	78 νCO + 8 νCN + 4 ρNCO	amide I′
1502			amide II
	1468	46 $\delta_{as}CH_3(N)$ + 16 $\delta_{as}CH_3(N)$ + 8 νCN + 4 δND	amide II′
1454	1454	69 $\delta_{as}CH_3(N)$ + 23 $\delta_{as}CH_3(N)$	
1446	1444	53 $\delta_{as}CH_3(C)$ + 18 $\delta_{as}CH_3(C)$	
1439	1426	68 $\delta_{as}CH_3(C)$ + 23 $\delta_{as}CH_3(C)$	
1384	1395	33 $\delta_{s}CH_3(N)$ + 16 νCN + 12 $\delta_{as}CH_3(N)$ + 10 δND	
1354	1352	88 $\delta_{s}CH_3(C)$	
1219			amide III
1120	1144	32 $\rho_{as}CH_3(N)$ + 15 δNR + 11 $\rho_{as}CH_3(N)$	
1106	1106	69 $\rho_{as}CH_3(N)$ + 23 $\rho_{as}CH_3(N)$	
1061	1082	44 νNR + 13 $\rho_{as}CH_3(C)$ + 11 δND	
1013	1013	54 $\rho_{as}CH_3(C)$ + 18 $\rho_{as}CH_3(C)$ + 16 πCO	
954	966	25 $\rho_{as}CH_3(C)$ + 24 νNR + 23 νCC	
	892	59 δND + 15 δNR	amide III′
831			amide IVa
	822	21 νCN + 20 δNR + 14 νCC + 11 δNCO	amide IV′a
601			amide VI
	583	73 πCO + 16 $\rho_{as}CH_3(C)$	amide VI′
593			amide IVb
	589	39 δNCO + 27 νCC + 18 δNR	amide IV′b
414			amide V
412			amide VII
	409	66 ρNCO + 12 δNR + 9 $\rho_{as}CH_3(C)$	amide VII′
	316	53 τCN + 29 πND + 10 πCO	amide V′
276			amide VIII
	273	55 δNR + 22 δNCO + 19 ρNCO	amide VIII′
154			amide IX
	156	65 πND + 25 τCN	amide IX′
71	76	50 τNR + 14 πND + 9 τCN	
45	49	62 τCC + 12 πCO + 7 τNR	

the increase in frequency of both fundamentals in the sequence given in Table 12 confirms this theory. On deuteration, the coupling between νCN and δNH is released, and we observe the amide II′, exhibiting high νCN character in the 1500 cm^{-1} region. The amide III′ band, with high δND character, is situated in the 900 cm^{-1} region. However, we must remark that in the deuterated compound the νCN and δND modes are still coupled but to a lesser extent than in the normal compound.

All secondary amides exhibiting a C−C amide bond show two bands, respectively, in the 800 cm^{-1} and 600 cm^{-1} region. Both bands have a high νCC and δNCO character and can be considered as typical "zone frequencies".

Generally the highest band is assigned as the νCC and the 600 cm^{-1} band as the δNCO mode or amide IV band. However, both bands are practically equally typical for this functional group, and both should be regarded as amide bands. Therefore, we propose to assign the 850 cm^{-1} band to the amide IVa and the 600 cm^{-1} band to the amide IVb. The amide IVa band also has a considerable νCN character. On deuteration, the amide IV′a and IV′b slightly shift to lower frequency and hardly change their character.

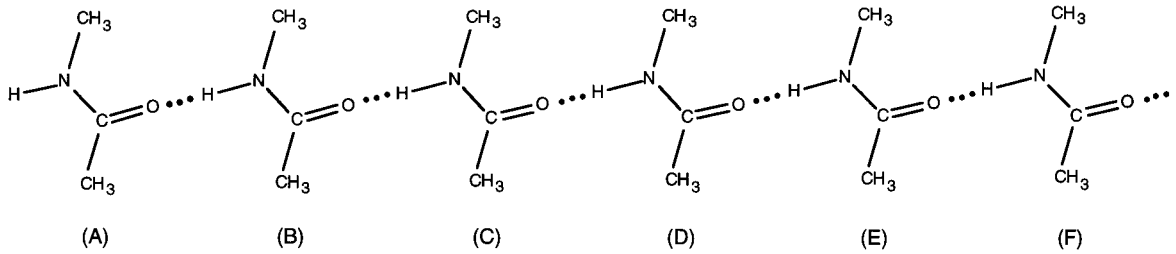

Figure 21. Geometry of NMA, $n = 6$.

TABLE 12: Influence of Hydrogen Bonding on the Amide Fundamentals

	monomer (calcd)	multimer ($n = 6$)	multimer ($n = 25$)[a]		solid (25 °C)	solid (−196 °C)
νNH	3456	3326	(3301)	IR	3304	3263
				R	3300	3256
amide I	1702	1651	(1645)	IR	1659	1643
				R	1651	1627
amide II	1502	1553	1559	IR	1566	1577
				R		
amide III	1219	1273	1277	IR	1301	1310
				R	1302	1320
amide IVa	831	854	856	IR	892	894
				R	883	894
amide IVb	593	596	596	IR	602	614
				R	609	616
amide V	414	573[b]	573	IR	725	792
				R		
amide VI	601	732[b]	743	IR	629	636
				R	628	635
amide VII	412	423	425	IR	439	440
				R	437	439
amide VIII	276	287	287	IR	290	318
				R	286	316
amide IX	154	185	187	IR	198	216
				R	188	224

[a] Extrapolated by decay curves. [b] PED changes drastically by the formation of multimers.

Strong coupling has been calculated between the πNH, πND, and τCN modes, resulting in bands at 414 cm^{-1} and 154 cm^{-1} for the normal compound and at 316 cm^{-1} and 156 cm^{-1} for N-deuterated NMA. The highest band has been assigned to the amide V band and considerably shifts to 316 cm^{-1} on deuteration (amide V′). Typical for this amide V band is the strong shift to higher frequency by stronger hydrogen bonding, and this is indeed observed from Table 12. The ratio amide V/amide V′ = 1.32 is typical for the amide V band.

The amide VI band with high πCO character is also generally observed in the 600 cm^{-1} region and appears less polarized than the amide IVb band in the aqueous Raman spectra. We calculated this amide VI band at 601 cm^{-1} for the normal compound and at 583 cm^{-1} for the deuterated NMA.

Also generally accepted is the amide VII mode with high ρNCO character and appearing in the 450 cm^{-1} region. This mode is calculated at 412 cm^{-1} and 409 cm^{-1} for the normal and deuterated compounds.

All those deformation modes are expected to shift to higher frequency by stronger hydrogen bonding. The calculation of these deformations for the multimers and the experimental data in the solid state confirm this statement.

Another typical band arising in the low-frequency region is the 276 cm^{-1}/273 cm^{-1} band exhibiting high δNR, δNCO, and ρNCO character for both the normal and deuterated compounds. These contributions are all situated in the secondary amide group and should therefore also be considered as a typical amide band. We propose to call the band the amide VIII band.

TABLE 13: Some Interatomic and Intermolecular Distances (Å) and Angles (deg) for the Optimized Geometry in the Monomer and Hexamer

		Monomer	Hexamer					
			at A	B	C	D	E	F
HN		1.0090	1.0096	1.0163	1.0181	1.0187	1.0183	1.0167
CN		1.3691	1.3583	1.3525	1.3513	1.3516	1.3530	1.3628
CO		1.2246	1.2326	1.2375	1.2387	1.2385	1.2372	1.2301
C=O···H–N	angle		174.35	173.78	173.04	173.62	173.39	
O·····H	distance		1.9324	1.8945	1.8846	1.8918	1.9299	

TABLE 14: Average Hydrogen Bond Energies for Different Multimers

number of hydrogen bonds	average hydrogen bond energy (kJ)
1	31.8
2	35.3
3	37.3
4	38.6
5	39.5
25	40.76[a]

[a] Calculated from $y = y_0 + a(1 - b^x)$.

The lowest observed and calculated band is situated in the 170 cm^{-1} region and exhibits, as already mentioned, a high τCN character coupled with πNH and πND modes. This band can be called the amide IX band.

12. Cooperative Effect in Hydrogen Bonding of NMA. To confirm the existence of the cooperative effect in NMA we calculated the monomer and the multimers with x varying between 2 and 6. The equilibrium geometry was calculated, without any structural restrictions. Subsequently, for all obtained equilibrium geometries, the vibrational frequencies and their infrared intensities were calculated using standard harmonic force fields.

In Figure 21 we present some data of the optimized geometry of the hexamer, and the data are collected in Table 13. From this table we can learn that, in the hydrogen bonding between molecules A and B, we only have to consider the pile-up effect in molecule A and the spill-over effect in molecule F.[32] This results in shorter CO and NH bonds and longer CN bonds compared with molecules B, C, D, and E where both the pile-up and spill-over effect occur.

The strong cooperative effect can also be shown by the average hydrogen bond energies defined as

$$\frac{E_{(trans-\mathrm{NMA})x} - xE_{(trans-\mathrm{NMA})}}{x - 1}$$

The data are collected in Table 14. The value obtained for the *trans*-NMA dimer (31.8 kJ mol^{-1}) compares favorably with the values of 26.0, 27.8, and 29.9 kJ mol^{-1} recently reported by H. Torii[92] and W. Qian.[93]

TABLE 15: Calculated Fundamentals (cm^{-1}) and Relative Intensities (in Parentheses) of Some Multimers of NMA

1	2	3	4	5	6
			νNH		
3456 (16)	3454 (21) 3407 (369)	3454 (24) 3386 (96) 3377 (905)	3454 (25) 3378 (366) 3371 (294) 3350 (1106)	3454 (25) 3374 (393) 3368 (369) 3345 (11) 3335 (1831)	3453 (26) 3370 (379) 3361 (350) 3343 (425) 3337 (37) 3326 (2292)
			amide I		
1702 (240)	1696 (8) 1682 (637)	1692 (140) 1682 (36) 1669 (1095)	1691 (142) 1682 (132) 1673 (1) 1661 (1601)	1690 (147) 1681 (105) 1674 (153) 1667 (2) 1656 (2092)	1689 (151) 1680 (122) 1673 (1) 1668 (266) 1662 (4) 1651 (2596)
			amide II		
1502 (129)	1530 (119) 1512 (168)	1545 (107) 1536 (176) 1515 (170)	1550 (62) 1547 (217) 1538 (175) 1515 (172)	1555 (13) 1552 (210) 1549 (232) 1538 (174) 1516 (173)	1558 (1) 1555 (50) 1553 (345) 1548 (222) 1542 (175) 1515 (175)
			amide III		
1218 (110)	1243 (131) 1232 (44)	1261 (102) 1246 (84) 1236 (62)	1267 (153) 1264 (5) 1248 (90) 1237 (62)	1271 (165) 1267 (10) 1265 (44) 1248 (46) 1238 (62)	1273 (209) 1270 (2) 1267 (38) 1265 (32) 1250 (91) 1238 (61)

These data show that, upon increasing the number of molecules, the average hydrogen bond energy increases from 31.8 kJ mol^{-1} in the dimer to 39.5 kJ mol^{-1} in the hexamer.

In agreement with the literature,[92] the data derived from the DFT calculations therefore clearly show that in the different multimers a strong cooperative effect is present. The existence of this cooperative effect can also be deduced from the calculated frequencies, which are for some fundamentals summarized in Table 15. These data indicate that, upon increasing the number of molecules, both the calculated hydrogen bond energies and the frequency shifts tend to converge to a constant value. Therefore, to obtain information on the asymptotic behavior of these properties, the calculated data were fitted using simple decay functions of the type

$$y = y_0 + a(1 - \mathrm{b}^*)\ (\Delta E)$$

$$y = y_0 + a\ \mathrm{e}^{-bx}\ (\nu\mathrm{NH},\ \text{amide I})$$

$$y = y_0 + a(1 - \mathrm{e}^{-bx})\ (\text{other amide bands})$$

with x being the number of hydrogen bonds in the complex species. The resulting functions, illustrating the asymptotic behavior as x increases from 0 to 25, is also shown in Figure 22 for the νNH and the amide I mode.

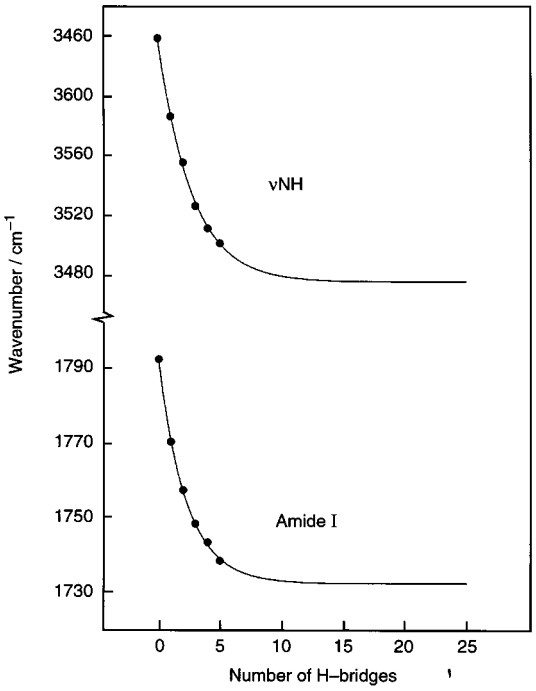

Figure 22. Asymptotic behavior of νNH and amide I modes as a function of the increasing number in the multimer.

Conclusions

Although an enormous amount of work has been published on the vibrational analysis of NMA, still a lot of contradictions and uncertainties about the vibrational spectra in the solid state existed. We have shown that a thorough infrared and Raman study of the solid state at different temperatures can resolve a lot of these uncertainties, taking into account the different structures at lower temperature, the shift and splitting of the bands due to the change in the hydrogen bonding, and the changes in the crystal structure.

The changes in the spectra on passing from the gas phase to the room temperature spectra and further to the low-temperature spectra can all be explained by assuming stronger intermolecular bonds in this series.

In the last part of the article we reexamined the typical trans secondary amide function and proposed the amide IVa and amide IVb bands as a coupling between the νCC and δNCO modes. We also proposed in the low-frequency region two new bands designated as the amide VIII and amide IX bands.

Furthermore, the cooperative effect has been nicely demonstrated by calculations of the fundamentals of the multimers and the average hydrogen bond energy.

Acknowledgment. The authors thank the FWO for financial support for the T.A. and spectroscopic equipment and Greta Thijs for technical assistance. W.A.H. thanks the FWO for an appointment as Postdoctoral Fellow.

References and Notes

(1) Wang, Y.; Portello, R.; Georgion, S.; Spiro, T. G. *J. Am. Chem Soc.* **1991**, *113*, 6368.
(2) Triggs, N. E.; Valentini, J. J. *J. Phys. Chem.* **1992**, *96*, 6922.
(3) Triggs, N. E.; Bonn, R. T.; Valentini, J. J. *J. Phys. Chem.* **1993**, *97*, 5535.
(4) Triggs, N. E.; Valentini, J. J. *Isr. J. Chem.* **1994**, *34*, 89.
(5) Mayne, L. C.; Hudson, B. *J. Phys. Chem.* **1991**, *95*, 2962.
(6) Song, S.; Asher, S. A.; Krimm, S.; Shaw, R. D. *J. Am. Chem. Soc.* **1991**, *113*, 1155.
(7) Fillaux, F.; Fontaine, J. P.; Baron, M. H.; Kearly, G. J.; Tomkinson, J. *Chem. Phys.* **1993**, *176*, 249.
(8) Barthes, M.; Bordallo, H. N.; Eckert, J. E., Maurus, O.; De Nunzio, G.; Leon, J. *J. Phys. Chem. B* **1998**, *102*, 6177.
(9) Boutin, H.; Yip, S. *Molecular spectroscopy with neutrons*; MIT Press: Cambridge, 1968; p 194.
(10) Fillaux, F.; Thompkinson, J. *Chem. Phys.* **1977**, *26*, 295.
(11) Bradbury, E. M.; Elliot, A. *Spectrochim. Acta* **1963**, *19*, 995.
(12) Araki, G. Suzuki, K.; Nakayama, H.; Ishii, K. *Phys. Rev.* **1991**, *43* (*15*), 12662.
(13) Balazs, A. *J. Mol. Struct.* **1987**, *153*, 103.
(14) Mirkin, N. G.; Krimm, S. *J. Mol. Struct.* **1991**, *242*, 143.
(15) Jakes, J.; Krimm, S. *Spectrochim. Acta* **1971**, *27A*, 19.
(16) Rey-Lafon, M.; Forel, M. T.; Garrigou-Lagrange, C. *Spectrochim. Acta* **1973**, *29A*, 471.
(17) Miyazawa, T.; Shimanouchi, T.; Mizushima, S. I. *J. Chem. Phys.* **1958,** *29*, 611.
(18) Nielsen, O. F.; Christensen, D. H.; Ramussen, O. M. *J. Mol. Struct.* **1991**, *242*, 273.
(19) Fillaux, F.; Baron, M. H.; De Loze, C.; Sagon, G. *J. Raman Spectrosc.* **1978**, *7* (5), 244.
(20) Jensen, J. H.; Christiansen, P. L.; Skovgaard, O.; Nielsen, O. F.; Bigio, I. J. *Phys. Lett. A* **1986**, *117*, 123.
(21) Kessler, H. K.; Sutherland, G. B. B. M. *J. Chem. Phys.* **1953**, *21*, 570.
(22) Barthes, M.; Ribet, M. *Biological macromolecular dynamics*; Cuiak, S., et al., Eds.; Adenine Press: Schenectady, NY, 1997.
(23) Frisch, M. J.; Trucks, G. W.; Schlegel, H. B.; Scuseria, G. E.; Robb, M. A.; Cheeseman, J. R.; Zakrzewski, V. G.; Montgomery, J. A.; Stratmann, R. E.; Burant, J. C.; Millam, J. M.; Daniels, A. D.; Kudin, K. N.; Strain, M. C.; Farkas, O.; Tomase, J.; Barone, V.; Cossi, M.; Cammi, R.; Mennucci, B.; Pomelli, C.; Adamo, C.; Clifford, S.; Ochterski, J.; Petersson, G. A.; Ayala, P. Y.; Cuis, Q.; Morokuma, K.; Malick, D. K.; Rabuck, A. D.; Raghavachari, K.; Foresman, J. B.; Cioslowski, J.; Ortiz, J. V.; Stefanov, B. B.; Liu, G.; Liashenko, A.; Piskorz, P.; Komaromi, I.; Gomperts, R.; Martin, R. L., Fox, D. J.; Keith, T.; Al-Laham, M. A.; Peng, C. Y.; Nanayakkara, A.; Gonzalez, C.; Challacombe, M.; Gill, P. M. W.; Jonhnson, B. G.; Chen, W.; Wong, W. M.; Andres, J. L.; Head-Gordon, M.; Replogle, E. S., Pople, J. A. *Gaussion 98*, Revision A.5; Gaussion, Inc.: Pittsburgh, PA, 1998.
(24) Becke, A. D. *J. Chem. Phys.* **1993**, *98*, 5648.
(25) Lee, C.; Yang, W.; Parr, R. G. *Phys. Rev. B* **1988**, *37*, 785.
(26) Katz, L.; Post, B. *Acta Crystallogr.* **1960**, *13*, 624.
(27) Itoh, K.; Shimanoschi, T. *Biopolymers* **1967**, *5*, 921.
(28) Desseyn, H. O.; Van der Veken, B. J.; Herman, M. A. *Spectrochim. Acta* **1977**, *33A*, 633.
(29) Desseyn, H. O.; Jacob, W. A.; Herman, M. A. *Spectrochim. Acta* **1972**, *28A*, 1329.
(30) Nyquist, R. A.; Chrisman, R. W.; Putzig, C. L.; Woodward, R. W.; Loy, B. R. *Spectrochim. Acta* **1979**, *35A*, 91.
(31) Lautie, A.; Froment, F.; Novak, A. *Spectrosc. Lett.* **1976**, *9* (5), 289.
(32) (a) Gutman, V. *The donor acceptor approach to molecular interactions*; Plenum Press: New York, 1978. (b) Gutman, V. *Rev. Chim. Roum.* **1977**, *22*, 679.
(33) Vinogradov, S. N.; Linell, R. H. *Hydrogen bonding*; Van Nostrand: New York, 1971.
(34) Ghosh, P. N. *J. Phys. C.: Solid state phys.* **1977**, *10*, 4421.
(35) Ambrose, E. J.; Elliot, A.; Temple, R. B. *Proc. R. Soc.* **1951**, *A206*, 192.
(36) Volkenstein, M.; Elyashevich, M. A.; Stepanov, B. I. *Zh. Fiz. Kim.* **1950**, *24*, 1153.
(37) Hexter, R. M.; Dows, D. A. *J. Chem. Phys.* **1956**, *25*, 504.
(38) Ratajczak, H.; Yaremko, A. M. *Chem. Phys. Lett.* **1999**, *314*, 122.
(39) Furer, V. L. *J. Mol. Struct.* **1997**, *435*, 151.
(40) Noda, I.; Lin, Y.; Ozaki, Y. *J. Phys. Chem.* **1996**, *100*, 8665.
(41) McQuade, D. T.; McKay, S. L.; Powell, D. R.; Gellman, S. H. *J. Am. Chem. Soc.* **1997**, *119*, 8528.
(42) Nielsen, O. F.; Bigio, I. J.; Olsen, I. *Chem. Phys. Lett.* **1986**, *132*, 502.
(43) Cheam, T. C.; Krimm, S. *J. Chem. Phys.* **1985**, *82*, 163.
(44) Dellepiane, G.; Abbate, S.; Bosi, P.; Zerbi, G. *J. Phys. Chem.* **1980**, *73*, 1040.
(45) Chen, X. G.; Schweitzer-Stenner, R.; Asher, S. A.; Mirkin, N. G.; Krimm, S. *J. Phys. Chem.* **1995**, *99*, 3074.
(46) Careri, G.; Buontempo, U.; Galluzi, F., Scott, A. C.; Gratton, E.; Shyamsunder, E. *Phys. Rev. B.* **1984**, *30*, 4689.
(47) Careri, G.; Buontempo, U.; Carta, F.; Gratton, E.; Scott, A. C. *Phys. Rev. Lett.* **1983**, *51*, 304.
(48) Eilbeck, J. C.; Lomdahl, P. S.; Scott, A. C. *Phys. Rev.* **1984**, *B30*, 4703.
(49) Alexander, D. M.; Krumhansc, J. A. *Phys. Rev.* **1986**, *B33*, 7172.
(50) Takeno, S. *Prog. Theor. Phys.* **1986**, *75*, 1.
(51) Johnson, C. T.; Swanson, B. I. *Chem. Phys. Lett.* **1985**, *114*, 547.
(52) Scott, A. C.; Bigio, I. J.; Johnston, C. T. *Phys. Rev.* **1989**, *B39*, 12883.
(53) Sauvajol, J. L.; Almairac, R.; Moret, J.; Barthes, M.; Ribet, J. L. *J. Raman Spectrosc.* **1989**, *20*, 517.
(54) Ataka, S.; Takeuchi, H.; Tasumi, M. *J. Mol. Struct.* **1984**, *113*, 147.
(55) Radzickal, A.; Pedersen, L.; Wolfenden, R. *Biochemistry* **1988**, *27*, 4538.
(56) Jorgensen, W. L.; Gao, J. *J. Am. Chem. Soc.* **1988**, *110*, 4212.
(57) Barker, R. H.; Boudreaux, G. J. *Spectrochim. Acta* **1967**, *23*, 727.
(58) Rees, D. C.; Lewis, M.; Honzatko, R. B.; Lipscomb, W. N.; Hardman, K. D. *Proc. Natl. Acad. Sci. U.S.A.* **1981**, *78*, 3408.
(59) Scherer, G. S.; Kramer, M. L.; Schutkowski, M.; Reimer, U.; Fischer, G. J. *Am. Chem. Soc.* **1998**, *120*, 5568.
(60) Li, P.; Chen, X. G.; Schulin, E.; Asher, S. A. *J. Am. Chem. Soc.* **1997**, *119*, 1116.
(61) Jones, R.; Smith, R. E. *J. Mol. Struct.* **1968**, *2*, 175.
(62) Venkatachalapathi, Y.; Mierke, B. F.; Taulane, J. P.; Goodman, M. *Biopolymers* **1987**, *26*, 763.
(63) Russel, R. A.; Thompson, H. W. *Spectrochim. Acta* **1956**, *8*, 138.
(64) Nyquist, R. A. *Spectrochim. Acta* **1963**, *19*, 509.
(65) Desseyn, H. O. *The chemistry of acid derivatives*; Patai, S., Ed.; J. Wiley & Sons: New York, 1992; Vol. *2*; p 292.
(66) Rey-Lafon, M.; Forel, M. T.; Garrigou-Lagrange, C. *Spectrochim. Acta* **1973**, *29A*, 471.
(67) Colaniani, S. E. M.; Nielsen O. F. *J. Mol. Struct.* **1995**, *347*, 257.
(68) Nielsen, O. F.; Lund, P. A.; Praestgaard, E. *J. Chem. Phys.* **1982**, *77*, 3678.
(69) Austin, J. C.; Jordan, T.; Spiro, T. G. In *Polymer Spectroscopy*; Clark, R. J. H., Hester, R., Eds.; Wiley: Chichester, 1993; pp 55−127.
(70) Johnson, S. W.; Eckert, J.; Barthes, M.; McMullan, R. K.; Muller, M. *J. Phys. Chem.* **1995**, *19*, 16293.
(71) Kutznetsova, L. M.; Furer, V. L.; Maklakov, L. I. *J. Mol. Struct.* **1996**, *380*, 23.
(72) Yarwood, Y. *Spectroscopy and structure of molecular complexes*; Plenum Press: London, 1973; pp 315−318.
(73) Lake R. F.; Thompson, H. W. *Proc. R. Soc. London* **1966**, *291(A)*, 469.
(74) Dako, G. P.; Gellman, S. H. *J. Am. Chem. Soc.* **1993**, *115*, 4228.
(75) Torii, H.; Tatsumi, T.; Tasumi, M. *J. Raman Spectrosc.* **1998**, *29*, 537.
(76) Popov, E. M.; Zheltova, V. N. *J. Mol. Struct.* **1971**, *10*, 221.
(77) Guo, H.; Karplus, M. *J. Phys. Chem.* **1992**, *96*, 7273.
(78) Han, W. G.; Suhai, S. *J. Phys. Chem.* **1996**, *100*, 3942.
(79) Jorgensen, W. L.; Swenson, C. J. *J. Am. Chem. Soc.* **1985**, *107*, 1489.
(80) Mitchell, J. B. O. *Chem. Phys. Lett.* **1991**, *180*, *6*, 517.
(81) Schellman, J. A. *C. R. Trav. Lab. Carlsberg, Ser. Chim.* **1955**, *29*, 223.
(82) Klotz, I. M. *Brookhaven Symp. Biol.* **1960**, *13*, 25.
(83) Akiyama, M.; Torii, H. *Spectrochim. Acta* **1994**, *A56*, 137.
(84) Chen, X. G.; Schweiter-Stenner, R.; Krimm, S., Irkin, N. G.; Asher, S. A. *J. Am. Chem. Soc.* **1994**, *116*, 11141.
(85) Kearly, G. J.; Fillaux, F.; Baron, M. H.; Bennington, S.; Thomkinson *Science* **1994**, *264*, 1285.
(86) Perrin, C. L. *Science* **1994**, *266*, 1665.

(87) Van Meervelt, L.; Bruyneel, C.; Morisse, H.; Zeegers-Huyskens, T. H. *J. Phys. Org. Chem.* **1997**, *10*, 825.
(88) Kessler, H. *Angew. Chem., Int. Ed. Engl.* **1982**, *21*, 512.
(89) Hallam, H. E. *Vibrational spectroscopy of trapped species*; Wiley: London, 1973.
(90) Schneider, B.; Horeni, A.; Pivcova, H.; Honzl, J. *Collect. Czech. Chem. Commun.* **1969**, *30*, 219.
(91) Keuleers, R.; Desseyn, H. O.; Rousseau, B.; Van Alsenoy, C. *J. Phys. Chem. A* **1999**, *103* (24), 4621.
(92) Torii, H.; Tatsumi, T.; Kanazawa, T.; Tasumi, M. *J. Phys. Chem. B* **1998**, *102*, 309.
(93) Qian, W.; Mirkin, N. G.; Krimm, S. *Chem. Phys. Lett.* **1999**, *315*, 125.